nature cancer

ARTICLES

https://doi.org/10.1038/s43018-021-00261-1

IRS1 phosphorylation underlies the non-stochastic probability of cancer cells to persist during EGFR inhibition therapy

Adi Jacob Berger[1,19], Elinor Gigi[1,19], Lana Kupershmidt[2,3], Zohar Meir[4,5], Nancy Gavert[1], Yaara Zwang[1], Amir Prior[6], Shlomit Gilad[7], Uzi Harush[8,9], Izhak Haviv[2,3,10], Salomon M. Stemmer[11], Galia Blum[12], Emmanuelle Merquiol[12], Mariya Mardamshina[13], Sivan Kaminski Strauss[14], Gilgi Friedlander[15], Jair Bar[16], Iris Kamer[16], Yitzhak Reizel[17], Tamar Geiger[13], Yitzhak Pilpel[14], Yishai Levin[6], Amos Tanay[4,5], Baruch Barzel[8,9], Hadas Reuveni[2,18] and Ravid Straussman[1]✉

Stochastic transition of cancer cells between drug-sensitive and drug-tolerant persister phenotypes has been proposed to play a key role in non-genetic resistance to therapy. Yet, we show here that cancer cells actually possess a highly stable inherited chance to persist (CTP) during therapy. This CTP is non-stochastic, determined pre-treatment and has a unimodal distribution ranging from 0 to almost 100%. Notably, CTP is drug specific. We found that differential serine/threonine phosphorylation of the insulin receptor substrate 1 (IRS1) protein determines the CTP of lung and of head and neck cancer cells under epidermal growth factor receptor inhibition, both in vitro and in vivo. Indeed, the first-in-class IRS1 inhibitor NT219 was highly synergistic with anti-epidermal growth factor receptor therapy across multiple in vitro and in vivo models. Elucidation of drug-specific mechanisms that determine the degree and stability of cellular CTP may establish a framework for the elimination of cancer persisters, using new rationally designed drug combinations.

Stochastic phenotypic cell transitions have been shown in multiple biological systems to facilitate the ability of a population to maintain equilibrium among different cell states. For example, when luminal, basal or stem-like subpopulations of breast cancer cells were enriched by sorting, they all returned to equilibrium proportions over time[1]. Chaffer et al. showed the ability of both normal and neoplastic cells to switch between stem-like and non-stem states[2]. Such cellular plasticity was also demonstrated in the ability of cancer cells to switch their phenotype between epithelial and mesenchymal states[3].

It has also been suggested that cancer drug-tolerant persisters can stochastically switch between two phenotypic states. Persisters have been described as a small subpopulation of quiescent cells that persist during drug therapy and, upon drug withdrawal, may give rise to a new population of cycling cells that are as sensitive to the drug as the original drug-naive population[4–6]. We refer to this new population of cells as drug-released persisters (DRPs). It has been shown that although the frequency of persisters can vary among cancer cell lines, it is highly stable over time within each cell line[6], suggesting that their frequency in the population is tightly regulated. However, the underlying mechanisms that regulate the frequency of persisters in a given population remain unclear. In particular, it is yet to be discovered whether this frequency and the transition between the states are controlled by inter-cellular crosstalk.

To uncover such potential mechanisms, we first sought to determine the rate by which persisters revert to their drug-sensitive phenotype. Previous reports have demonstrated the reversibility of the persisters' phenotype by testing the half-maximum inhibitory concentration (IC_{50}) of growth inhibition after several days of drug withdrawal and comparing it to that of the drug-naive population. While IC_{50} is indeed a measurement of drug potency[7], it reflects predominantly the effect of the drug on cellular proliferation and does not directly measure either cell killing or the frequency of persisters.

Here we demonstrate that although the IC_{50} of growth inhibition is indistinguishable between DRPs and the drug-naive population as previously suggested[6], DRPs retain a higher frequency of

[1]Department of Molecular Cell Biology, Weizmann Institute of Science, Rehovot, Israel. [2]TyrNovo Ltd, Rehovot, Israel. [3]Cancer Personalized Medicine and Diagnostic Genomics Lab, Azrieli Faculty of Medicine in the Galilee, Bar-Ilan University, Safed, Israel. [4]Department of Biological Regulation, Weizmann Institute of Science, Rehovot, Israel. [5]Department of Computer Science and Applied Mathematics, Weizmann Institute of Science, Rehovot, Israel. [6]De Botton Institute for Protein Profiling, The Nancy and Stephen Grand Israel National Center for Personalized Medicine, Weizmann Institute of Science, Rehovot, Israel. [7]The Nancy and Stephen Grand Israel National Center for Personalized Medicine, Weizmann Institute of Science, Rehovot, Israel. [8]Department of Mathematics, Bar-Ilan University, Ramat-Gan, Israel. [9]Gonda Multidisciplinary Brain Research Center, Bar-Ilan University, Ramat-Gan, Israel. [10]AID Genomics and Gensort Ltd, Rehovot, Israel. [11]Davidoff Center, Rabin Medical Center, Felsenstien Medical Research Center, Petach Tikva, and Sackler Faculty of Medicine, Tel Aviv University, Tel Aviv, Israel. [12]Institute of Drug Research, The School of Pharmacy, Faculty of Medicine, Campus Ein Karem, The Hebrew University, Jerusalem, Israel. [13]Department of Human Molecular Genetics and Biochemistry, Sackler School of Medicine, Tel Aviv University, Tel Aviv, Israel. [14]Department of Molecular Genetics, Weizmann Institute of Science, Rehovot, Israel. [15]Ilana and Pascal Mantoux Institute for Bioinformatics, The Nancy and Stephen Grand Israel National Center for Personalized Medicine, Weizmann Institute of Science, Rehovot, Israel. [16]Sheba Medical Center, Ramat Gan, Israel. [17]Department of Genetics and Institute for Diabetes Obesity and Metabolism, Perelman School of Medicine, University of Pennsylvania, Philadelphia, PA, USA. [18]Purple Biotech Ltd, Rehovot, Israel. [19]These authors contributed equally: Adi Jacob Berger, Elinor Gigi. ✉e-mail: ravidst@weizmann.ac.il

persisters for an extended period of time. A detailed study of the mechanisms that may account for the higher frequency of persisters in DRPs led us to suggest a model according to which every cancer cell in the population has a highly stable CTP during drug therapy. According to this model, CTP, rather than being a discrete property of a subpopulation of cells, is continuously distributed across the entire population, in a unimodal rather than a bi-modal distribution. We also found that the CTP of a cell is heritable and may be different under different drugs. Accordingly, we demonstrate that the higher frequency of persisters observed in DRPs is the result of the enrichment of cancer cells with relatively higher CTP by drug treatment. We thus report that, unlike many other cellular phenotypic states that regain their original frequency in the population following a perturbation, the persistence phenotype is selected over time and therefore drives a non-genetic mechanism of tumor evolution. Furthermore, we found that the stable cellular memory of the CTP is encoded by the phosphorylation status of insulin receptor substrate 1 (IRS1) and we demonstrate, using multiple in vivo models, that inhibition of IRS1 is highly synergistic with epidermal growth factor receptor (EGFR) inhibition. Overall, we suggest that modulation of the long-term memory of cellular CTP can lead to new approaches to eliminate persisters.

Results

DRPs have a higher frequency of persisters than drug-naive cells. It has been demonstrated that upon drug withdrawal cancer persisters give rise to a new population of cells that are as sensitive to the drug as the original drug-naive population[4–6]. To uncover the kinetics by which persisters, upon drug release, return to their original frequency within the overall cancer cell population, we first generated DRPs by treating drug-naive cells from the EGFR-mutated lung cancer cell line PC9 with 0.5 μM of the EGFR inhibitor gefitinib for 9 d and then let the cells proliferate without the drug for an additional 6 weeks. We then compared the percentage of persisters in DRPs versus drug-naive cells. We discovered that after 9 d of treatment with gefitinib, PC9 DRPs had 4.2-times more persisters than the naive population (36% versus 8.5%, respectively; Fig. 1a–c). Note, that previous studies assessed the sensitivity of naive cells and of DRPs to EGFR inhibition based on their IC_{50} after 72 h of gefitinib treatment and not by direct measurement of the frequency of persisters. As the majority of PC9 cells die more than 72 h after the initiation of drug treatment (Fig. 1c and Supplementary Videos 1–3), this early measurement reflects mostly the effect of the drug on growth rate, rather than on cancer cells killing and on the resulting frequency of persisters[7] (Extended Data Fig. 1). We also found, as previously reported, that the dose–response curve of naive PC9 cells and of DRPs was identical when measured after 72 h of drug treatment[6] (Fig. 1d).

To check the generality of our observation, we tested both the IC_{50} and the frequency of persisters in three additional human cancer cell lines treated with clinically relevant drugs. The HCC2935 lung adenocarcinoma cell line, harboring an EGFR activating mutation, was treated with gefitinib; the G361 melanoma cell line, harboring a V600E BRAF activating mutation, was treated with the MEK inhibitor trametinib; and the SKBR3 breast adenocarcinoma cell line, which overexpresses HER2, was treated with the EGFR/HER2 dual inhibitor lapatinib (Supplementary Tables 1 and 2). We found that the increase in the frequency of persisters in the DRP population was observed in all three cell lines, despite no significant change in the IC_{50} of DRPs of these cell lines (Fig. 1e,f). This observation is in sharp contrast to antibiotic-released bacterial persisters, which were shown to give rise to a population that has a similar persister frequency as the parental population[8,9]. The high frequency of persisters in cancer DRPs was maintained for at least 10 weeks (>40 doublings) of a drug holiday (Extended Data Fig. 2a), suggesting a long-lasting increase in the frequency of persisters in DRPs.

CTP is a continuous trait and is enriched by drug treatment. To better understand the mechanisms underlying the higher frequency of persisters in DRPs, we tested whether we could isolate and expand rare persister cells from the naive population. We generated 544 and 408 single-cell-derived clones from PC9 and the melanoma cell line G361, respectively, and tested their frequency of persisters after 7 d of drug treatment. Notably, we did not identify a discrete, narrowly defined subpopulation of persisters, but rather a continuum of clones displaying a broad range of drug survival, which we termed CTP (Fig. 2a,b). We also generated an additional 43 single-cell-derived clones from the PC9-naive population, for which we measured both IC_{50} after 72 h of gefitinib treatment and CTP after 7 d of treatment. We found again a continuum of CTP values, with no correlation to clonal IC_{50} values (Fig. 2c and Extended Data Fig. 2b). As expected by the apoptotic nature of EGFR inhibitor-induced cell death, clones with low CTP had higher percent of cells with cleaved caspase 3 under gefitinib treatment as compared to clones with high CTP (Extended Data Fig. 2c). To rule out the possibility that high-CTP clones are resistant to gefitinib treatment, we showed that these clones (1) have the same high CTP under afatinib and osimertinib, second and third-generation EGFR inhibitors that inhibits the most common mechanism of resistance to gefitinib, the T790M mutation in EGFR (Fig. 2d and Extended Data Fig. 2d)[10–12] and (2) that clones with high CTP continue to die over time, as expected of drug-tolerant rather than of drug-resistant cells that are able to proliferate under therapy[13] (Fig. 2e).

The higher frequency of persisters in DRPs than in naive cells can be explained by enrichment of cells with pre-existing high CTP following drug treatment, by drug-induced changes in cell-intrinsic CTP or by both. To directly measure the distribution of CTP in DRPs, we generated 392 and 265 additional single-cell-derived clones from both PC9 and G361 DRPs, respectively. We found that CTP distribution of DRP clones was shifted to the right, toward higher CTP, compared to the distribution of naive clones (Fig. 2f,g). Modeling of the shift expected by mere enrichment of cells with higher CTP was enough to explain most of the shift observed by the experimental data, suggesting that the higher frequency of persisters in DRPs is attributed mostly to the enrichment of cells with higher CTP by treatment (Extended Data Fig. 2e,f). As drug-tolerant cells continue to die under drug treatment (Fig. 2e) we hypothesized that the longer cells are treated before the drug holiday, the greater the selection for higher CTP cells will be and the resulting DRPs will also have higher CTP. Indeed, we found a positive correlation between length of treatment used for generating DRPs and CTP (Fig. 3a). Last, we hypothesized that if high CTP clones are enriched by drug treatment, multiple cycles of drug treatment and drug holiday will select for cells with higher CTP with each of the treatment cycles. Indeed, we observed a steep rise in the CTP of PC9 DRPs undergoing one, two or three cycles of drug treatment (Fig. 3b).

CTP is heritable and does not correlate with doubling time. To better characterize stability of the clonal CTP trait, we repeatedly tested the CTP of drug-naive PC9 clones with varying CTP values for up to 18 weeks of propagation in drug-free medium. We found that clonal CTP remained stable over this period (Fig. 3c). When we generated single-cell-derived sub-clones from two clones with high CTP (clone 4 and clone B12) the CTP values of the sub-clones were spread around the CTP of the parental clonal population (Fig. 3d). We conclude that, despite a wide range of CTPs across cancer cells in the population, the CTP is a heritable trait and thus highly stable over time at the clonal level.

Although it has been suggested that persisters are quiescent or slow-cycling cells[4,6,14], both in our 544 PC9 clones and 408 G361 clones, we found that the CTP trait does not correlate with clonal population doubling time or with the time that it took us to generate the clones from single cells (Extended Data Fig. 3a–f). Detailed

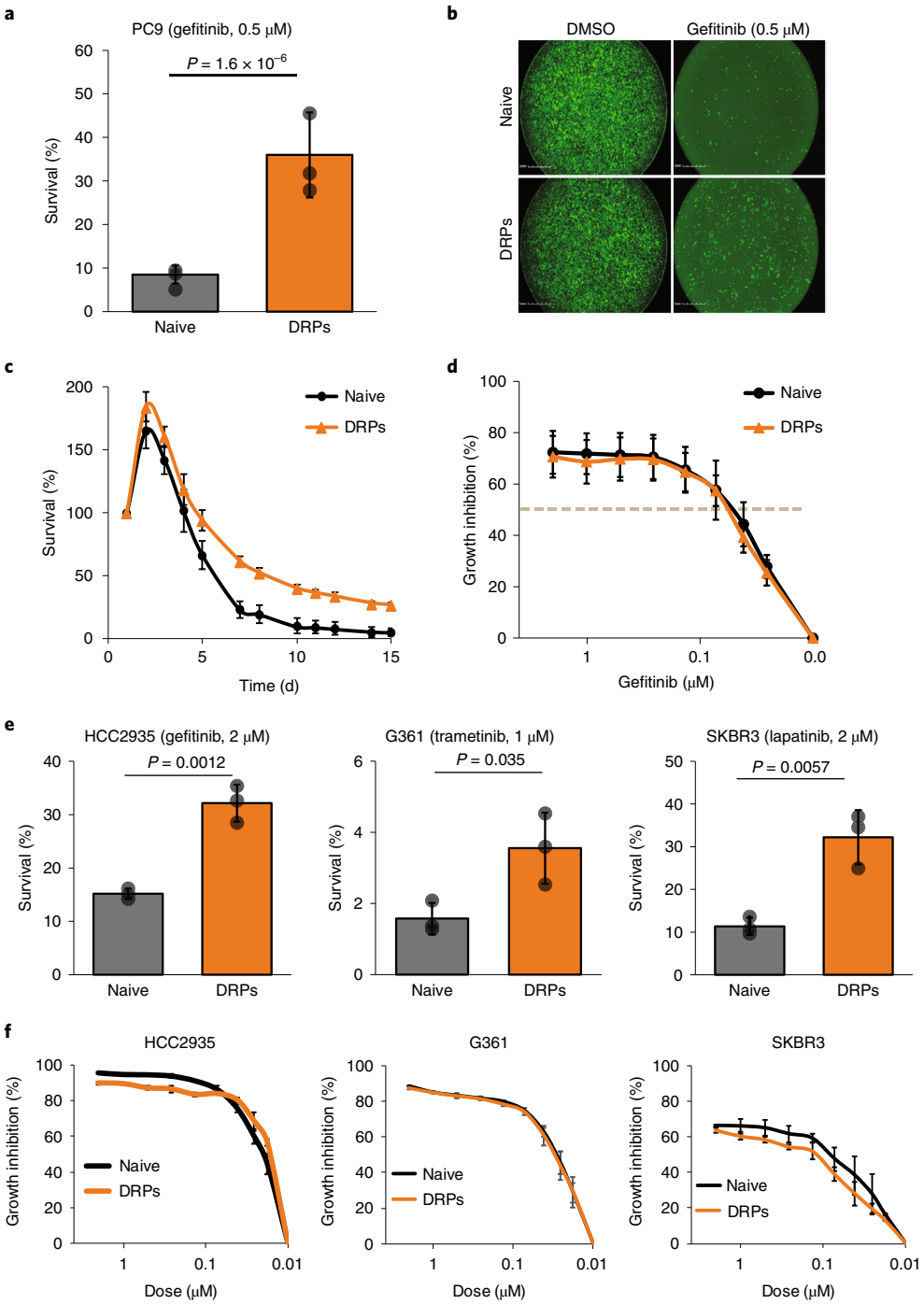

Fig. 1 | DRPs have higher frequency of persisters than the drug-naive population. a, Percentage of persisters after 9 d of gefitinib treatment is shown for both PC9 drug-naive cells and DRPs. DRPs were generated by treating PC9 drug-naive cells with 0.5 μM gefitinib for 9 d and then growing them without drug for additional 6 weeks (6-week DRPs). To measure survival after 9 d of treatment with 0.5 μM gefitinib, 6,000 cells per well of either drug-naive cells or 6-week DRPs were plated in 96-well plates and counted by microscopy at different time points. Survival was calculated by the percentage of cells that survived at the end of the experiment (day 9) out of the number of cells that were present in the well just before drug treatment (day 1). Data are presented as mean values and error bars represent s.d. of $n = 3$ independent cultures. **b**, Representative images of GFP-positive PC9-naive cells and 6-week DRPs after 9 d of DMSO or gefitinib treatment. **c**, PC9 drug-naive cells or 4–7-week DRPs were treated for 15 d with 1 μM gefitinib. Cells were counted by microscopy and their number was normalized to the cell number before treatment. Data are presented as mean values and error bars represent s.d. of $n = 8$ independent cultures. **d**, Dose–response curve after 72 h of drug treatment for GFP-positive PC9 drug-naive cells or 6-week DRPs. GFP intensity values were normalized to DMSO control. Data are presented as mean values and error bars represent s.d. of $n = 4$ independent cultures. **e**, Percentage of persisters after 9 d of gefitinib treatment is shown for drug-naive cells and 5–6-week DRPs from HCC2935, G361 and SKBR3 cell lines, treated with the indicated drugs and concentrations. Data are presented as mean values and error bars represent s.d. of $n = 3$ independent cultures. **f**, Dose–response curve after 72 h of drug treatment for G361, SKBR3 and HCC2935 drug-naive cells or DRPs, as indicated. Data are presented as mean values and error bars represent the s.d. of $n = 3$ independent cultures. Statistical significance (**a**,**e**) was assessed using a two-tailed Student's *t*-test.

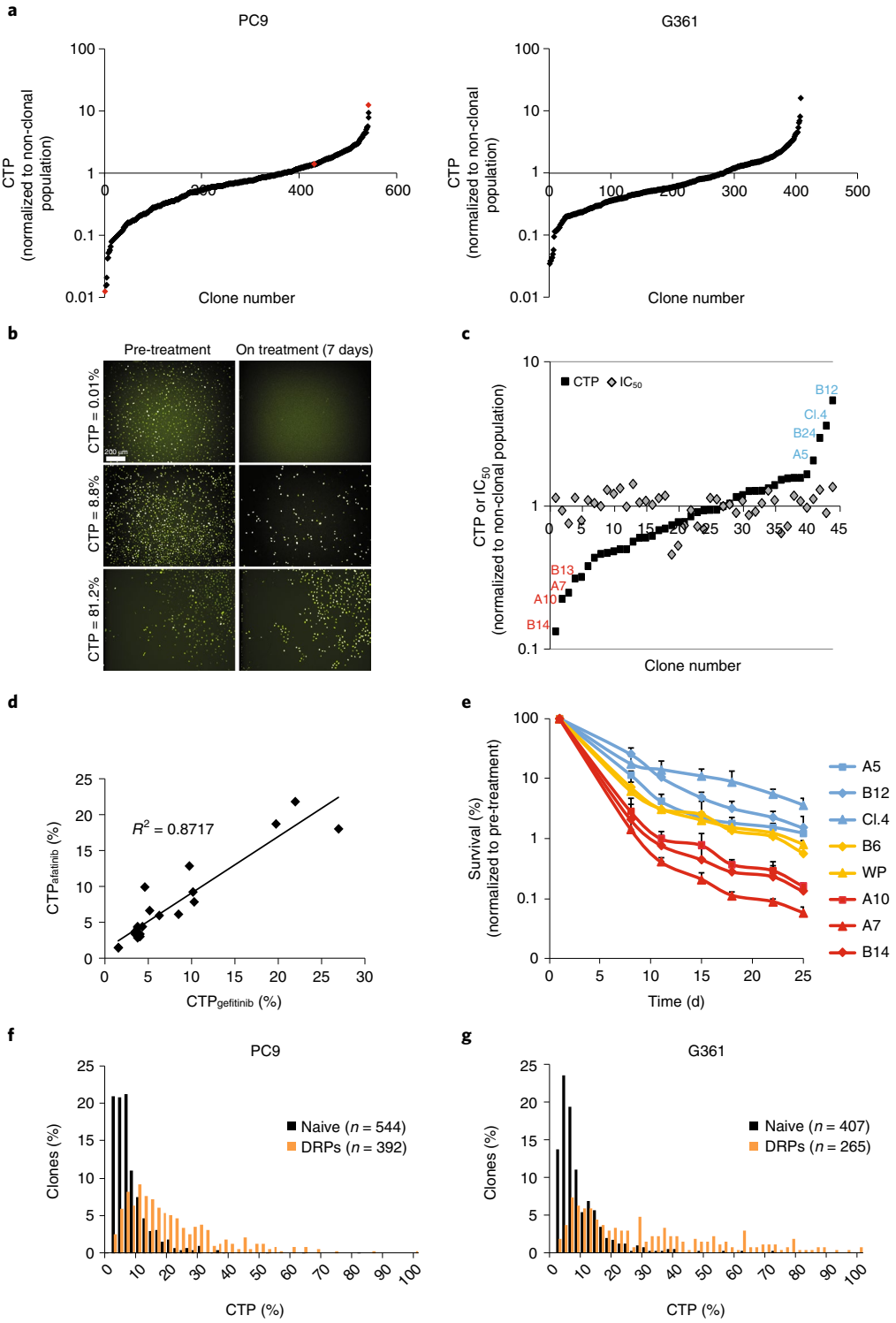

Fig. 2 | CTP is a continuous trait and is enriched by drug treatment. a, Single-cell-derived clones of yellow fluorescent protein (YFP)-positive PC9 ($n = 544$ clones) and G361 ($n = 408$ clones) cell lines were grown for 12–20 d, then treated with gefitinib and trametinib, respectively, for 7 d. The CTP of each clone was normalized to the average CTP of all clones (6.7% and 8.3%, respectively), which represent the CTP of the non-clonal population. **b**, Images of the three PC9 clones that are marked in red in **a**. **c**, Single-cell-derived clones of a GFP-positive PC9 cell line ($n = 43$ clones) were grown to ~10 million cells. The CTP and IC_{50} of each clone were tested after 7 d and 72 h of treatment with gefitinib, respectively and were normalized to the naive non-clonal population. The names of eight of the clones are shown. **d**, Scatter plot demonstrating correlation between $CTP_{gefitinib}$ and $CTP_{afatinib}$ after 7 d of treatment for 20 PC9 clones and the PC9 non-clonal population. **e**, Seven PC9 clones and the non-clonal population were treated with 0.5 µM gefitinib for 25 d. The percentages of remaining cells (compared to the number of cells pre-treatment) are presented for each clone. Colors indicate the clonal CTP; blue, high CTP clones; yellow, average CTP clones; red, low CTP clones. Data are presented as mean values and error bars represent s.d. of $n = 3$ independent cultures. **f**,**g**, CTP histogram of drug-naive cells and DRPs from PC9 (**f**) and G361 (**g**) cell lines. DRPs were generated by 9 d of treatment and 6 weeks of drug holiday. CTP was measured after 7 d of treatment.

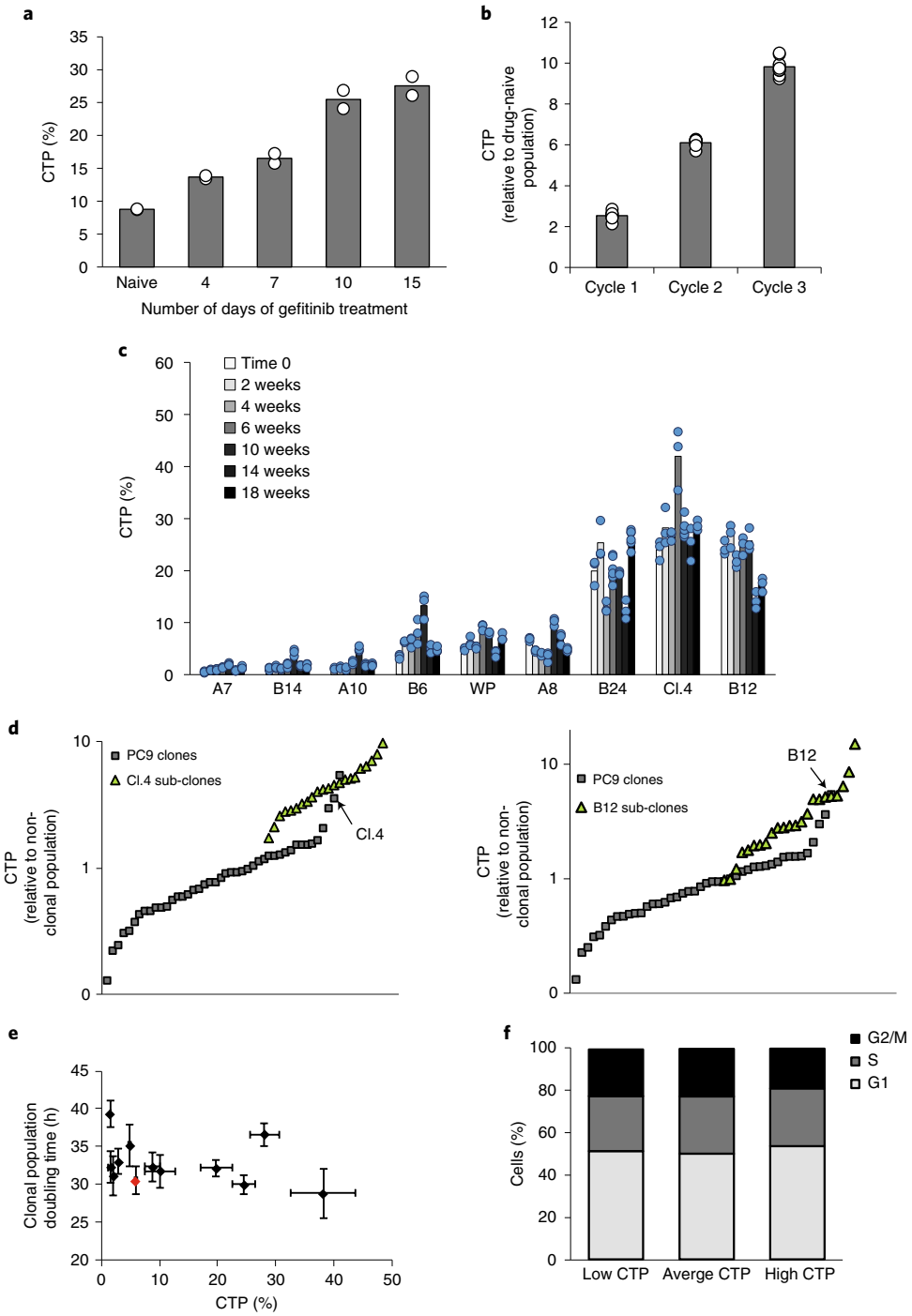

Fig. 3 | CTP is a heritable trait that does not correlate with cell cycle status. a, Percentage of persisters after 7 d of 0.5 μM gefitinib treatment is shown for both PC9 drug-naive cells and DRPs that were generated by treating PC9 drug-naive cells for 4–15 d with 0.5 μM gefitinib and then releasing the cells from drug for additional 2–3 weeks until cells regained their normal proliferation rate. Data are presented as mean values of $n = 2$ independent cultures with ten technical repeats each. **b**, Percentage of persisters after 7 d with 0.5 μM gefitinib, normalized to PC9 drug-naive population, is shown for PC9 DRPs generated by one, two or three cycles of 0.5 μM gefitinib treatment for 7 d followed by a drug holiday for 2–3 weeks until cells regained their normal proliferation rate. Data are presented as mean values of $n = 10$ technical repeats. **c**, Eight PC9 drug-naive clones, as well as the naive non-clonal population (WP), were grown for 18 weeks in drug-free medium. $CTP_{gefitinib}$ after 9 d of treatment was tested at the indicated times on a subset of cells derived from each clone. Data are presented as mean values and error bars represent s.d. of $n = 3$ technical repeats. **d**, The $CTP_{gefitinib}$ after 7 d of treatment of 22 or 23 single-cell-derived sub-clones of PC9 clone 4 (Cl.4) or clone B12, respectively (marked by an arrow), are shown on the background of the $CTP_{gefitinib}$ of the original 43 PC9 single-cell clones. **e**, Correlation across 11 PC9 clones and the non-clonal population (marked in red), between $CTP_{gefitinib}$ after 7 d of treatment and doubling time. Data are presented as mean values and error bars represent s.d. of $n = 3$ independent cultures. **f**, Cell cycle distribution of PC9 clones with low ($n = 4$ clones), average ($n = 3$ clones) or high ($n = 4$ clones) CTP. Results represent the mean values of $n = 2$ technical repeats of all clones in each group.

analysis of cell cycle status and clonal population doubling time of 11 PC9 clones with variable CTPs also confirmed the lack of correlation between CTP and doubling time or cell cycle status (Fig. 3e,f and Extended Data Fig. 3g). The difference between our results and previous reports probably stems from the fact that, traditionally, persisters were studied while on treatment[4–6,15–17]. Indeed, when a population enriched with persisters was isolated before treatment, these cells had a similar growth rate to that of the non-enriched population[18,19].

CTP is drug specific. To explore whether persisters are pan-drug tolerant[6,14] or drug specific, we measured the CTP of 45 PC9 drug-naive clones treated with 18 anticancer drugs for which PC9 cells were found to be sensitive. We found that different clones had a wide range of CTP with respect to all drugs that were tested (Fig. 4a–d and Extended Data Fig. 4a) and we found no clones that had high CTP with respect to all drugs. Rather, we found that clonal CTP was generally drug specific (Fig. 4e). The highest correlations of clonal CTPs were found between drugs with a similar target (Fig. 4e,f). Generally, we show that there is a higher correlation between clonal CTPs of cytotoxic–cytotoxic drug pairs than of targeted–targeted or targeted–cytotoxic pairs (Fig. 4e,g). To validate the drug-specific nature of DRPs in an additional lung cancer cell line, we used gefitinib to generate DRPs from the HCC2935 cell line and tested the percent of persisters of both HCC2935 drug-naive cells and DRPs that were treated with multiple drugs. We found that while HCC2935 DRPs had a significantly higher CTP when re-treated with gefitinib or with other targeted therapies, they generally had a lower CTP when treated with cytotoxic therapies (Extended Data Fig. 4b). These findings suggest that cancer persisters show some level of pan-drug resistance only in the context of cytotoxic therapies but a more target-specific persistence under different targeted therapies. They also suggest that different molecular mechanisms may account for cell-specific CTP with respect to different drugs.

Looking for a mechanism that determines $CTP_{gefitinib}$. To dissect the molecular mechanism that may account for stable CTP distribution in populations of cancer cells, we used $CTP_{gefitinib}$ as a model. Although single genetic alterations such as deletions, insertions and single-nucleotide polymorphisms are commonly found as drivers of drug resistance, the continuous nature of CTP distribution steered us away from looking for such binary alterations. Because PC9 cells are known to have multiple chromosomal rearrangements[20], we first examined the karyotype of ten cells from seven PC9 clones with varying $CTP_{gefitinib}$ values but could not detect any correlation with clonal $CTP_{gefitinib}$ (Extended Data Fig. 5a–c). We also could not detect any morphological changes that correlated with clonal $CTP_{gefitinib}$ values or any morphological changes between drug-naive cell lines and their DRPs (Extended Data Fig. 5d,e).

We subjected eight PC9 clones with highly variable $CTP_{gefitinib}$ to proteomic analysis, antibody array of apoptotic proteins and bulk RNA sequencing (RNA-seq), but could not find any protein or transcript that correlated with $CTP_{gefitinib}$ (Supplementary Tables 3–5). Although ALDH1A1, CD133, FGFR1, insulin-like growth factor 1 receptor (IGF1R), EGFR and NGFR have been previously suggested as biomarkers for persisters in different cancer models[4,6,15,18,19,21,22], we did not detect a significant correlation between their expression level and $CTP_{gefitinib}$ (Extended Data Fig. 6a). We also did not detect a difference in phosphorylated EGFR (pEGFR) between low and high CTP clones (Extended Data Fig. 6b).

To increase statistical power, we subjected 194 PC9 clones to messenger RNA sequencing (MARS-seq), both before and 24 h after gefitinib treatment and measured their proliferation rate and $CTP_{gefitinib}$ (Extended Data Fig. 7a–c and Supplementary Table 6). We found a strong proliferation signature that varied between clones but did not associate with CTP (Extended Data Fig. 7d–g). A screen for single genes that correlate with CTP predominantly revealed genes that are weakly, but significantly anti-correlated, including the *MUC5B* gene, which was previously shown to be correlated with a favorable outcome of patients with EGFR-mutated non-small cell lung cancer (NSCLC)[23] (Extended Data Fig. 7h–k). Positively correlated genes included the cancer stem cell marker ALDH1A3, a family member of ALDH1A1, which was previously shown to have a role in maintaining persister survival and resistance[18,24] (Extended Data Fig. 7l). As these genes explained only a small part of CTP variability, we looked for gene modules that are correlated with CTP. We found one such module, the mucin module, which includes *MUC1* and *MUC20*, among other genes (Extended Data Fig. 8). Although the correlation of this module with CTP was highly significant after gefitinib treatment, it was not statistically significant before treatment and therefore cannot explain the stable pre-set probability of PC9 cells to persist during EGFR inhibition therapy (Extended Data Fig. 8e).

Next, we sought to find drugs with a known mechanism of action that can modulate the percentage of persisters and may direct us to the mechanism that controls $CTP_{gefitinib}$. We assembled a library of 523 drugs and tested for their direct effect on PC9 cells as well as for their effect on the percentage of persisters after 7 d of treatment with 1 μM gefitinib. Of the 25 drugs that reduced the percentage of persisters to gefitinib (z score < -1.5) without decreasing the proliferation rate (z score > -1), we found multiple inhibitors of the IGF1R and of its downstream effectors, PI3K and PKC (Extended Data Fig. 6c and Supplementary Table 7). Although these results are consistent with the report by Sharma et al.[6] that activation of IGF1R helps persisters maintain viability under gefitinib treatment, we found no significant correlation between the expression or phosphorylation of IGF1R and $CTP_{gefitinib}$ among PC9 drug-naive clones (Extended Data Fig. 6a,d). We also did not find any correlation between the phosphorylation of IGF1R or EGFR in PC9 DRPs that were generated by treating drug-naive cells with gefitinib for 4, 7, 10 or 15 d (Extended Data Fig. 6e). We therefore concluded that although activation of IGF1R may indeed contribute to persistence during gefitinib treatment, cell-specific $CTP_{gefitinib}$ is probably encoded downstream of IGF1R, rather than by IGF1R expression or activity level pre-treatment. As IGF1R and many of its downstream effectors convey their signaling by phosphorylation reactions, we next looked for the mechanism that encodes the CTP by unbiased phosphoproteomics profiling.

$CTP_{gefitinib}$ correlates with S/T phosphorylation along IRS1. We first subjected seven drug-naive PC9 clones with $CTP_{gefitinib}$ values ranging from 2.1% to 89%, as well as the parental non-clonal

Fig. 4 | CTP is drug specific. a–d, Single-cell-derived clones of PC9 ($n = 43$ clones) as well as the non-clonal population were treated with the indicated drugs and concentrations for 7 d: BI6727, 2.5 μM, PLK inhibitor (**a**), WZ4002, 0.5 μM, EGFR inhibitor (**b**), 5-FU, 400 μM, thymidylate synthase inhibitor (**c**) and doxorubicin, 1 μM, intercalating agent (**d**). CTP of each clone was normalized to the CTP of the non-clonal population. For each drug, clones are ordered based on their CTP. **e**, The CTP of each 45 PC9 single-cell-derived clones was measured with respect to 18 anticancer drugs. The correlation matrix shows Pearson's correlation coefficient of the CTP vis-à-vis each pair of drugs. **f**, Scatter plots demonstrating the CTP of 45 PC9 clones under drugs with a similar mechanism of action after 7 d of treatment. Pearson's correlation R^2 coefficients and their Benjamini–Hochberg adjusted P values (P_{adj}) are presented for each graph. **g**, Scatter plots demonstrating the CTP of 45 PC9 clones treated for 7 d with each of the two indicated drug treatments. 5-FU, fluorouracil.

population, to an unbiased phospho-proteomic analysis. We detected more than 15,000 phospho-sites in more than 3,707 different proteins. Notably, we found that four of the 15 most correlated phospho-sites, including the top hit, serine residue 1101 (S1101), were serine/threonine (S/T) phospho-sites that belonged to IRS1 (Fig. 5a and Supplementary Table 8). IRS1 is an adaptor protein that transmits signals from IGF1R to the MAPK and PI3K/AKT pathways[25]. While tyrosine phosphorylation of IRS1

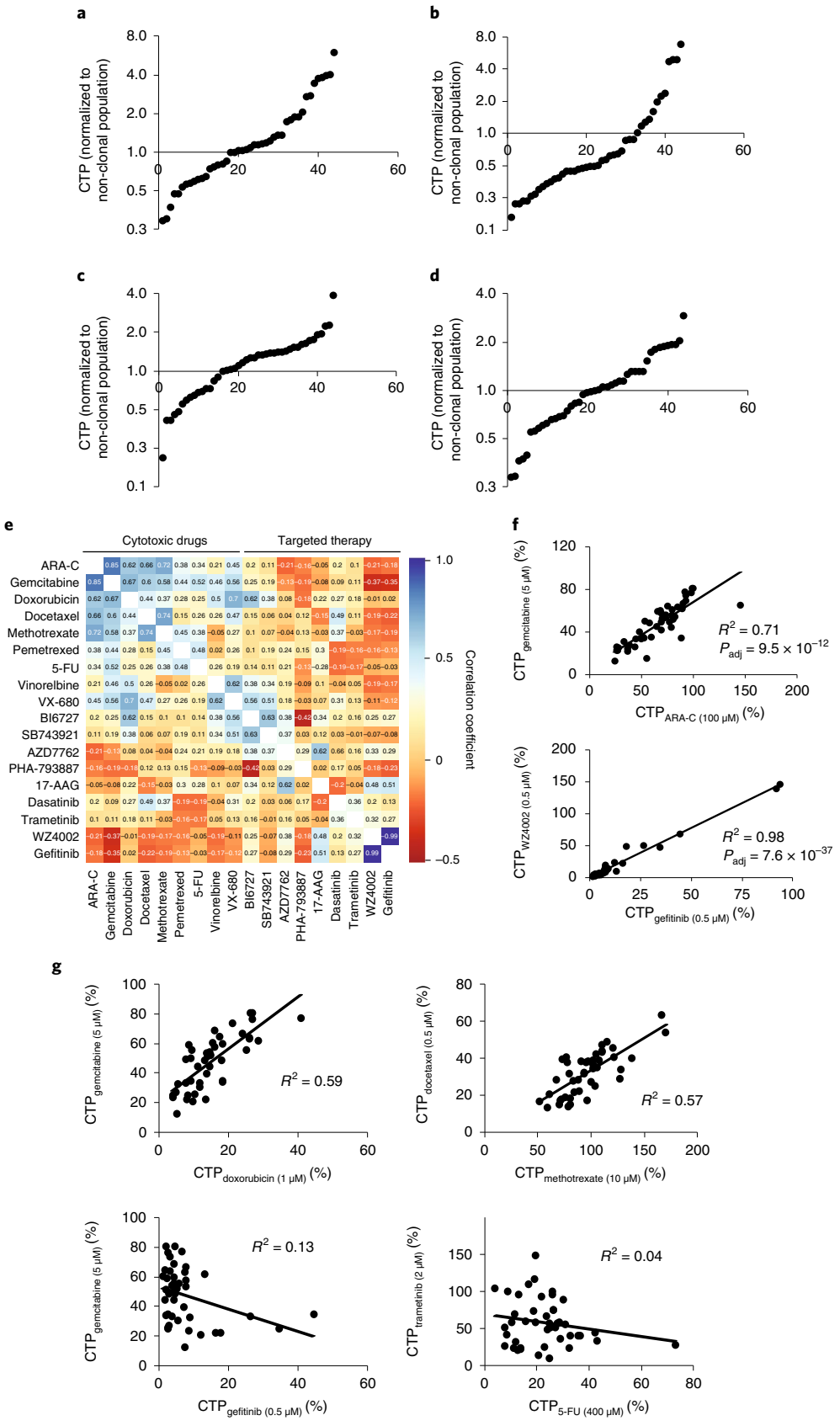

and its homolog protein, IRS2, by IGF1R or the insulin receptor is needed for their activation, S/T phosphorylation on the IRS1/2 tail region inhibits their activity[26]. Indeed, IRS1/2 S/T phosphorylation leads to dissociation of IRS1/2 from receptors and targets IRS1/2 for degradation[25]. Therefore, our results suggest a model in which IGF1R is activated in all PC9 cells upon EGFR inhibition, as suggested previously[6,27], but transmits the signal downstream more effectively in high CTP clones in which IRS1 S/T phosphorylation is low, enabling efficient signal transmission through IRS1 (Fig. 5b).

In agreement with this model, we found that multiple S/T phosphorylation sites along IRS1 were significantly correlated with CTP (Fig. 5c and Extended Data Fig. 9a). All the phosphorylation sites along IRS1 were negatively correlated with CTP, suggesting higher S/T phosphorylation and thus higher IRS1 inhibition in low CTP clones. This significant correlation was not observed in S/T sites of IRS2, which in general showed higher S/T phosphorylation irrespective of CTP. (Fig. 5d and Extended Data Fig. 9a). As expected from the highly stable nature of CTP (Fig. 3c), we found that the correlation between pIRS1 ser1101 and CTP was maintained in PC9 clones for at least 20 weeks of culture (Fig. 5e). Moreover, we show that DRPs of G361 and HCC2935 cell lines treated with the MEK inhibitor trametinib and gefitinib, respectively, had a significant reduction of S/T phosphorylation in ser1101 and Ser1078 of IRS1 (Fig. 5f and Extended Data Fig. 9b), consistent with the increase in CTP in DRPs (Fig. 1e). To demonstrate that cancer cells with low IRS1 S/T phosphorylation in a human tumor may be enriched by treatment, we cultured fresh slices from a human EGFR-mutated NSCLC tumor ex vivo and measured IRS1 ser1101 by immunohistochemistry (IHC) after 5 d of treatment with gefitinib or with dimethylsulfoxide (DMSO) control. We found that whereas a large variation in pIRS1 was detected in cancer cells in DMSO-treated slices, most cancer cells that survived gefitinib treatment were pIRS1 negative (Fig. 5g). Last, to show that pIRS1 levels correlate with treatment response in vivo, we turned to head and neck squamous cell carcinoma (HNSCC), as EGFR is overexpressed in up to 90% of HNSCC cases and is commonly treated with EGFR inhibitors[28–30]. We stratified 12 patient-derived xenografts (PDXs), obtained from HNSCC patient biopsies with EGFR amplification, based on their pIRS1 ser1101 levels pre-treatment. Eight tumors had a low pIRS1 score and four tumors had a high pIRS1 score. In agreement with our model, we found that PDXs with higher levels of pIRS1 showed a better response to cetuximab (Fig. 5h,i). Our results demonstrate that the phosphorylation status of S/T sites along IRS1 is highly correlated with the response to EGFR inhibition therapy.

Inhibition of IRS1 is synergistic with anti-EGFR therapy. Our model predicts that the potential of IRS1 to transmit IGF1R signaling serves as a functional bottleneck that controls the cellular CTP. Consistent with this model, we show that whereas overexpression of IRS1 in the naive PC9 population caused a marked elevation in gefitinib persister frequency (Fig. 6a), knocking down IRS1 in two high CTP clones by siRNA reduced the frequency of gefitinib persisters (Fig. 6b). Additionally, treatment of PC9 cells with tumor necrosis factor (TNF)-α, which was shown to inhibit IRS1 by phosphorylating multiple serines along its tail[31], caused an up to 13-fold decrease in the number of PC9 persisters (Fig. 6c). It should be noted that phosphorylation of IRS1 by TNF-α is only one of multiple effects that TNF-α may have on the cells. To directly test the effect of the phosphorylation of serines along IRS1 on CTP, we mutated nine of these serine residues into alanine, to prevent the potential phosphorylation of these residues. The serine residues that we chose to mutate were selected from the ten serine residues that we previously found to have a negative correlation between their phosphorylation status and CTP (Extended Data Fig. 9a). In agreement with our hypothesis we found that overexpression of IRS1 (9S → 9A) in two low CTP clones caused a larger increase in CTP as compared to overexpression of wild-type (WT) IRS1 (Fig. 6d). We also demonstrate that inhibition of pERK in response to gefitinib treatment was significantly greater in low than in high CTP clones (Fig. 6e), further supporting our model of stronger signaling downstream of IGF1R/IRS1 in high CTP clones. To show the effect of co-targeting IRS1 with EGFR in tumor cells we used the first-in-class IRS1 inhibitor NT219 (ref. [32]), which triggers serine phosphorylation and subsequent degradation of IRS1 (refs. [33,34]). We started with the National Cancer Institute H1975 NSCLC cell line, which harbors both the EGFR exon 21 activating mutation L858R, as well as the EGFR gatekeeper T790M mutation, which confers resistance to first generation EGFR inhibitors such as gefitinib. We found that combining the third-generation EGFR inhibitor osimertinib with NT219 resulted in a highly synergistic activity (Fig. 7a). To demonstrate the effect of co-targeting IRS1 and EGFR in tumors, we first treated ex vivo fresh slices of EGFR-mutated NSCLC PDX model TM00199 with gefitinib, NT219 or with both. We found a significant reduction in tumor cell viability when both EGFR and IRS1 were inhibited relative to the inhibition of either of the drugs alone (Fig. 7b). To show the effect of inhibiting IRS1 on the response to EGFR inhibition in vivo, we generated a PDX model from a bone marrow metastasis-derived biopsy of a 61-year-old patient with NSCLC with an EGFR exon 19 deletion and T790M mutation, who progressed on treatment with afatinib and with the third-generation EGFR inhibitor osimertinib before accrual of the biopsy. We found

Fig. 5 | Phosphorylation of multiple serine/threonine sites along IRS1 correlates with CTP during EGFR inhibition. a, Scatter plot demonstrating pIRS1 (ser1101) and $CTP_{gefitinib}$ after 7 d of treatment for seven PC9-naive clones as well as the non-clonal population. Pearson's correlation test was used to calculate the correlation coefficient and *P* value ($n = 2$ independent cultures for clones with 2.9%, 5.9%, 8.9%, 19.7% and 89% CTP; $n = 3$ independent cultures for clones with 2.1%, 24.5% and 86% CTP). **b**, Model showing effect of IRS1 S/T phosphorylation on CTP. In low CTP cells, high S/T phosphorylation blocks IRS1 activity, but in high CTP cells, the absence of IRS1 S/T phosphorylation enables IGF1R signaling to drive persistence under therapy. **c**,**d**, The six most phosphorylated S/T sites are presented for both IRS1 (**c**) and IRS2 (**d**). Black bars represent the mean of two clones with high CTP and gray bars represent the mean of two clones with low CTP. Pearson's correlation coefficients and their *P* values between the phosphorylation of each site and CTP are shown for each site. Bars represent the s.d. of $n = 5$ independent cultures from two clones. **e**, Scatter plot demonstrating pIRS1 (ser1101) and $CTP_{gefitinib}$ after 7 d of treatment for five PC9-naive clones as well as in the non-clonal population. The CTP was tested 20 weeks after clones were established and propagated in drug-free medium ($n = 2$ independent cultures for clone with 19.7% CTP; $n = 3$ independent cultures for clones with 2.9%, 5.9%, 8.9%, 24.5% and 86% CTP). **f**, pIRS1 (ser1101) and pIRS1 (ser1078) were measured in drug-naive cells and DRPs of the HCC2935 cell line treated with 0.5 μM gefitinib. Data are presented as mean values and error bars represent s.d. of $n = 3$ independent cultures. *P* value <0.05, by one-tailed Student's *t*-test. **g**, Fresh human NSCLC tumor was cut into 250-μm-thick slices and treated ex vivo with gefitinib or with DMSO control. After 5 d of treatment, slices were fixed and IHC was used to detect pIRS1 (ser1101). Three representative regions in the tumor are presented for each condition. Scale bar, 20 μm. **h**, Tumor growth inhibition of $n = 12$ HNSCC PDX models separated, based on their pIRS1 ser1101 levels. Dots represent the response of each PDX model treated with cetuximab for more than 3 weeks. Average inhibitions are marked in red lines. *P* value was calculated by one-tailed Student's *t*-test. **i**, IHC of pIRS1 ser1101 levels pre-treatment in eight representative PDX models, obtained from biopsies from patients with HNSCC with EGFR amplification. Scale bars, 30 μm (top), 100 μm (bottom).

that addition of NT219 to osimertinib resulted in a clear synergistic effect and tumor regression (Fig. 7c; Bliss score = 0.23). To demonstrate the synergistic effect of inhibiting IRS1 and EGFR in an additional cancer type, we generated a PDX model from a biopsy of a primary HNSCC in the salivary gland of a 40-year-old patient who had a known EGFR amplification. We found that a short treatment of 9 d with either cetuximab as a single treatment or cetuximab combined with NT219, resulted in remarkable regression of all tumors, whereas NT219 as monotherapy had no effect on tumor growth. Yet, tumors that were treated with NT219 and cetuximab showed significantly delayed recurrence upon treatment withdrawal compared to cetuximab alone ($P < 0.01$ by analysis of variance (ANOVA)), suggesting that the frequency of persisters was lower in the combination arm (Fig. 7d).

Discussion

It is now well appreciated that persisters are not merely a common cause of incomplete response to anticancer therapies, but can also evolve to clinically relevant drug-resistant cells[10,35,36]. Understanding the molecular mechanisms that underlie persisters and finding ways

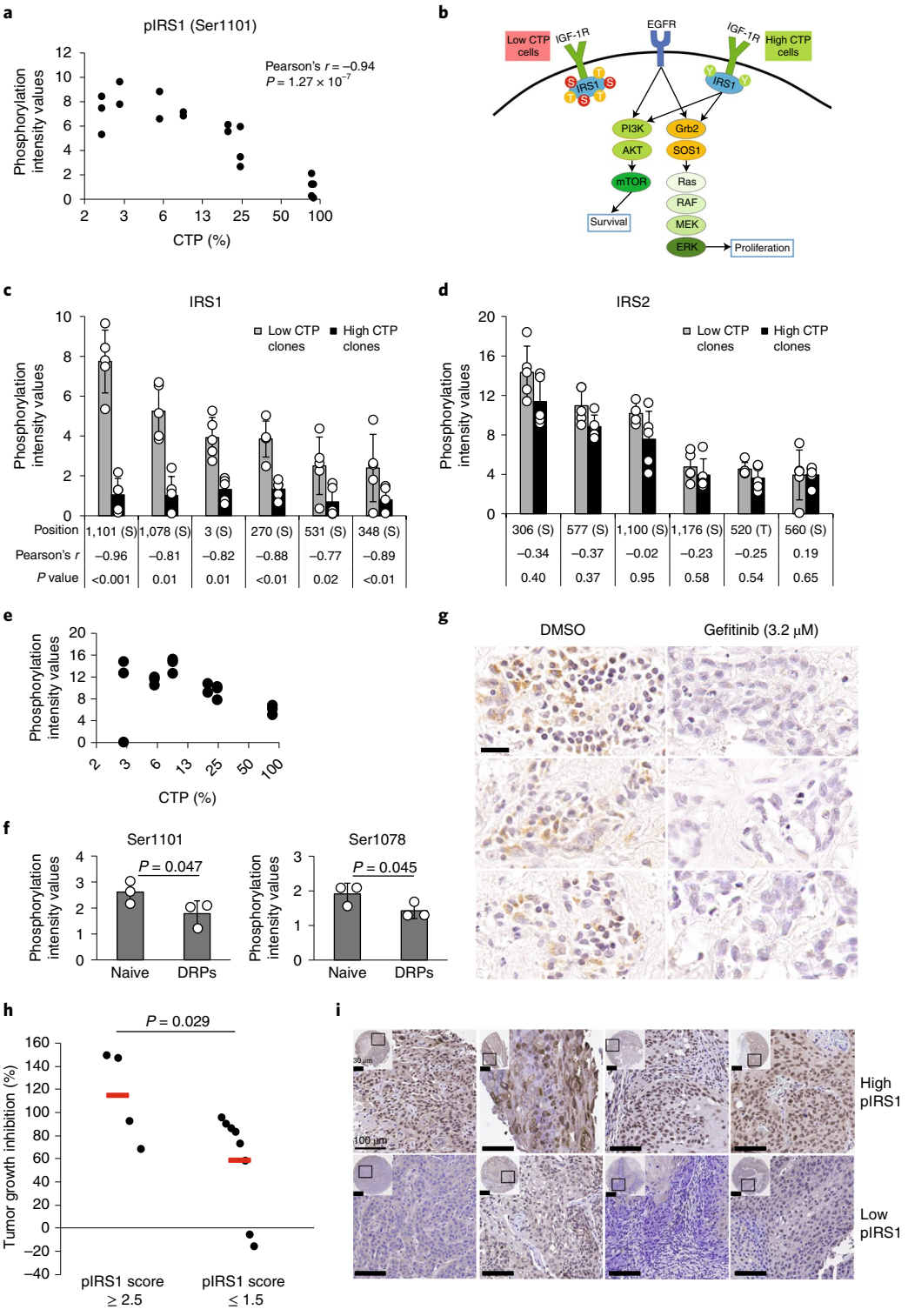

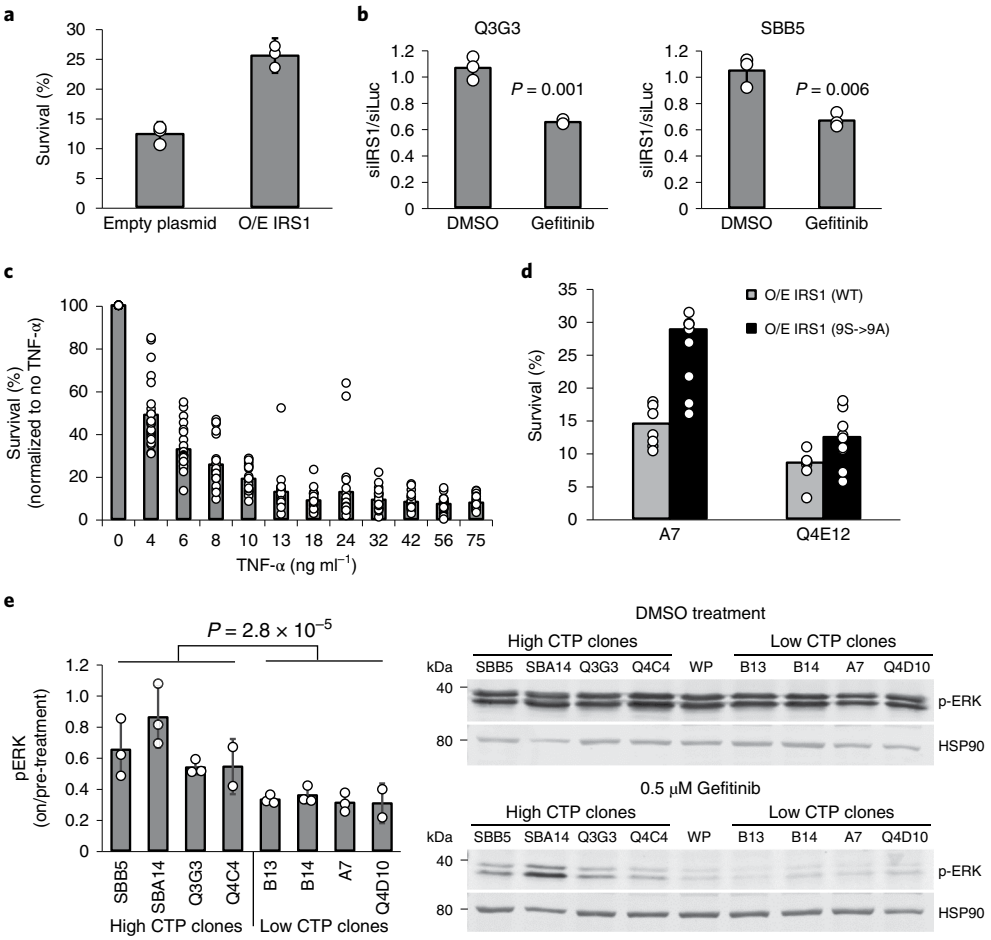

Fig. 6 | IRS1 modulation affects response to EGFR inhibition. a, The effect of overexpressing (O/E) human IRS1 or empty-vector control on $CTP_{gefitinib}$ of PC9 non-clonal population after 7 d of treatment. Data are presented as mean values and bars represent s.d. of $n=3$ independent cultures. **b**, The effect of targeting IRS1 with siRNA on $CTP_{gefitinib}$ was measured in two high $CTP_{gefitinib}$ clones treated with 0.35 μM gefitinib or with DMSO for 7 d. Results were normalized to the effect of siRNA against luciferase. Data are presented as mean values and bars represent s.d. of $n=3$ independent cultures. **c**, GFP-positive PC9 cells were plated on 384-well plate and treated with the designated concentrations of TNF-α, or with DMSO control and with 1 μM gefitinib. The number of cells after 6 d of treatment after each TNF-α dose was normalized to number of cells left with no TNF-α addition. Data are presented as mean values of $n=24$ technical repeats. **d**, The effect of overexpressing WT IRS1 or 9S → 9A IRS1 (Methods provides details of mutated sites) on $CTP_{gefitinib}$ was measured in two low CTP clones treated with 0.35 μM gefitinib or with DMSO for 7 d. Data are presented as mean values of $n=10$ technical repeats. **e**, Quantification and representative blot of pERK protein levels after 6 h of gefitinib treatment normalized to DMSO treatment. Data are presented as mean values and error bars represent s.d. from independent cultures ($n=2$ for clones Q4C4 and Q4D10; $n=3$ for clones SBB5, SBA14, Q3G3, B13, B14 and A7). Statistical significance for **a**, **b** and **d** was obtained using a two-tailed Student's *t*-test.

to eliminate them have consequently been the focus of many studies in the past decade[5,6,15–19,21,37–47].

While some studies described persisters as a small subpopulation of quiescent cells[6,48], Raha et al. reported that MET-amplified gastric cancer cells that are tolerant to MET inhibition have the same growth rate as non-tolerant cells[18]. Similarly, Shaffer et al. demonstrated that drug-tolerant melanoma cells are cycling rather than resting before drug treatment[19]. We also found no correlation between CTP and proliferation rate. Note, however, that our study is based on generating clones from single cells and it is therefore expected to miss non-cycling cells, as these would not generate clones. Therefore, our results neither support nor contradict the presence of an additional small subpopulation of non-cycling cells that have high CTP.

One of the hallmarks of cancer persisters, similar to bacterial persisters, was suggested to be their tendency to give rise, upon drug holiday, to a population that is as sensitive to therapy as the drug-naive population[4–6]. We found, however, that DRPs have a higher frequency of persisters than the drug-naive population. We hypothesize that this difference stems from the fact that previous reports measured the IC_{50} of DRPs while we measured the frequency of persisters directly. There are a few disadvantages in using IC_{50} as a proxy for persister rate: (1) IC_{50} is often calculated by testing the performance of each drug dose compared to non-treated control to obtain the dose–response curve from which one can extract the IC_{50}. When the measured phenotype is cell number, the IC_{50} represents the effect of the drug on both growth rate and cell death. As opposed to IC_{50}, persisters are measured by comparing the number of cells that remain viable after treatment to the number of cells that were present when drug treatment was applied. By doing so, we ignore the growth inhibition effect and focus mainly on the cell death effect (Extended Data Fig. 1). (2) IC_{50} is usually measured after 48–72 h of treatment. Here again, as growth inhibition is a much faster process than cell death induction, 72 h is often not enough time to induce massive cell death, therefore it is not suited for testing the frequency of persisters and better represent the effect of drugs on growth inhibition (Fig. 1c). (3) While IC_{50} is measured by testing multiple drug concentrations, persisters are measured

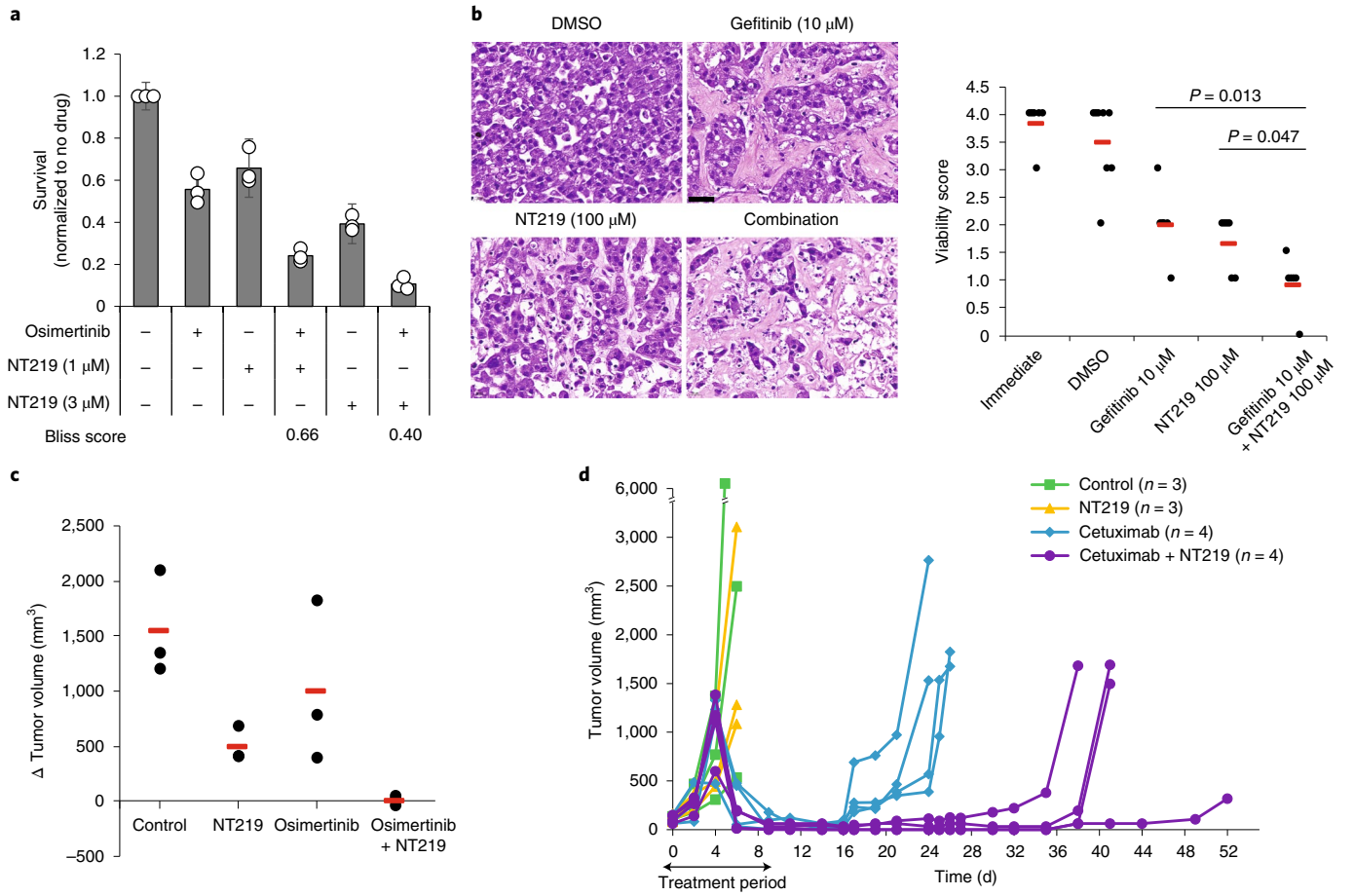

Fig. 7 | Inhibition of IRS1 is synergistic with anti-EGFR therapy. a, The effect of adding NT219 to 0.03 μM osimertinib on cancer cell viability was tested in National Cancer Institute H1975 NSCLC cell line after 7 d of treatment. Results were normalized to a no-treatment control. Bliss score <0.6 represents a synergistic effect. Data are presented as mean values and bars represent the s.d. of $n = 3$ independent cultures. **b**, The effect of adding NT219 to gefitinib was tested using ex vivo live slices of the TM00199 EGFR-mutated (L858R) NSCLC PDX model. Experiments were performed on $n = 6$ tumor slices originating from different regions in two PDX tumors. Dots represent the viability score ascribed by a pathologist. Average score marked in red. *P* value was obtained by a two sided Mann–Whitney *U*-test. Scale bars, 40 μm. **c**, The effect of adding NT219 to osimertinib was tested in vivo on EGFR(T790M)-mutated NSCLC PDX model. NT219 (65 mg kg^{-1} intravenously) and/or osimertinib (5 mg kg^{-1} orally) were administered twice and five times, respectively on the first week and once on day 15. The difference in tumor volumes between the end of the study (day 17) and day 1 is presented. Bliss score of 0.23 suggests a strong synergism between the drugs. **d**, PDX mice generated from a HNSCC human tumor were treated with cetuximab (1 mg per mouse on days 0, 4, 6 and 9), NT219 (65 mg kg^{-1} on days 0, 2, 4, 6 and 9) or both. Mice administered vehicle or NT219 alone were killed on day 6 following aggressive tumor progression. All tumors of the remaining groups (cetuximab and cetuximab + NT219) regressed and were followed for additional 43 d after treatment cessation. Mice were killed following tumor recurrence when tumor volume exceeded 1,500 mm^3.

for a specific drug concentration that should be far above the IC_{50}. Indeed, we demonstrated that there is no correlation between clonal IC_{50} and clonal CTP. Although it is common for cancer research papers to assess the activity of drugs after 48–72 h of treatment, our results should strongly motivate researchers to extend drug-efficacy assays well beyond these early time points.

Many studies have suggested that relatively short-term transcriptional variability of different proteins (for example, BIM, EGFR, AXL, NGFR, FGFR, TRAIL, AURKA, BCL-xL/BCL-2) can affect the chance of cancer cells to persist during therapy[5,10,19,21,22,42–44,46]. By contrast, our results demonstrate that clone-specific CTP is highly stable over many months. We speculate that single-cell transcriptional variability may indeed play a role in transiently increasing or decreasing the CTP from the stable clonal-specific CTP baseline.

The observation that CTP is a continuous and highly stable trait may have important clinical implications. First, it predicts that repeated cycles of treatment and drug holiday will select cells with higher CTP over time, as we have shown (Figs. 1a,b,e, 2f,g and 3b). Killing as many cancer cells as possible in the first rounds of treatments by higher-combination treatments or by reducing cell-specific CTP, may result in better long-term control of the disease, as we have demonstrated (Fig. 7d). Moreover, although the rate of cancer cell killing over the first few days of treatment is governed predominantly by the mean of the CTP distribution within cancer cells, it is the range of this distribution that governs the decay of the population over a prolonged period of time (Extended Data Fig. 10). As noted above, at present, the common practice is to evaluate therapeutic approaches based on their impact after 2–4 d. An additional disadvantage of this approach is that such short-term evaluation captures only the mean CTP and disregards the potentially slow long-term decay, driven by the CTP distribution. Therefore, a seemingly more effective treatment A may, in the long term, be outperformed by an initially inferior treatment B (Extended Data Fig. 10).

Our results also suggest that CTP is drug specific and that cells are usually not pan-drug tolerant. Moreover, we found that the correlation between the CTP of different cells in a population under

different drugs can be highly variable. As expected, the chance of cells to persist two drugs with a similar mechanism of action was highly correlated (Fig. 4f). Yet, we found that, generally, there is no correlation between the CTP of cells under cytotoxic and targeted therapies (Fig. 4e,g). We hypothesize that sequential treatments or combinations of drugs with non-correlated or anti-correlated CTP may have an advantage, as each of the drugs will eliminate most of the cells with a high chance to persist treatment with the other drug.

The drug specificity of CTP implies that different mechanisms must account for the chance of cells to persist during treatments with different drugs. We used persisters of lung cancer cells to EGFR inhibition as a model to discover the type of mechanism that underlies the uniquely continuous but stable CTP phenotype of these cells. The high stability of clonal CTP over months in culture cannot be readily explained by transient expression changes, as single-cell gene expression was shown to hold little memory over long periods and to display highly transient fluctuations[42,49]. Indeed, we found that the phosphorylation status of the IGF1R downstream effector IRS1 determines the cell-specific CTP by controlling the potential of IGF1R to emit its signaling and protect cells from EGFR inhibition therapy (Fig. 5b). The notion that protein phosphorylation can store long-term cellular memory has been demonstrated before, mostly in neurological studies, in which synaptic long-term memory was shown to be controlled by the phosphorylation of certain proteins[50–52]. Moreover, long-term effects, like insulin resistance in type 2 diabetes and brain dysfunction in Alzheimer's disease, have been shown to be affected by the S/T phosphorylation status of IRS1 (refs. [53–55]). Our findings thus, reveal another case of long-term cellular memory (cellular CTP), which is controlled by protein phosphorylation status.

The molecular mechanistic basis that controls continuous but stable pIRS1 status is yet to be uncovered. Although long-term cellular memory may indicate a genetic mechanistic basis, the continuous nature of CTP distribution across cells suggests that it is probably not controlled by a discrete single genetic change. Rather, pIRS1 status may be dictated by the net effects of multiple genetic changes. Unfortunately, we believe that our study was not sufficiently powered to reveal the nature of such multifactorial genetic inheritance by exome sequencing, as PC9 cells are genetically highly unstable[20]. Alternatively, epigenetic mechanisms may control the stable and non-stochastic continuous S/T phosphorylation status of IRS1. Additional studies are needed to uncover such genetic or epigenetic mechanisms that control pIRS1 and the CTP.

It is widely accepted that large intratumor variability exists between such cancer cell phenotypes as metastatic potential, stemness properties and response to drug therapy[6,56,57]. It remains to be elucidated how much of this variability is stable over time at the single-cell level and how much of it can be explained by post-translational modifications, such as phosphorylation.

Our study demonstrates that the chance of cancer cells to persist therapy varies greatly between cells, but it is highly stable at the clonal level. Our results show that persisters do not give rise to drug-sensitive cells but rather are selected by therapy. As a result, with repeated cycles of therapy, the population is becoming less sensitive to drugs, regardless of the selection of pre-existing or de novo genetic resistance mechanisms. Modulating drug-specific CTP or using higher-combination treatments may be a prerequisite for better disease control.

Methods

Cell lines and reagents. HCC2935 (American Type Culture Collection (ATCC), no. CRL-2869), G361 (ATCC, no. CRL-1424), SKBR3 (ACTT, no. HTB-30) and EFM192A (DSMZ, no. ACC 736) were grown in RPMI1640 (Biological Industries, no. 01-100-1A). The PC9 and NCI-H1975 cell lines were a gift from C. Yu of the Broad Institute of Harvard and MIT and were grown in DMEM (Invitrogen, no. 10569-010). Both growing media were supplemented with 10% FBS and 1% penicillin–streptomycin, pyruvate and glutamine (Invitrogen, no. 15140-122). Cell line authentication by fingerprinting analysis was performed for SKBR3, PC9 (non-clonal population) and two PC9 high CTP clones (Cl.4 and B12) to confirm their identity.

Whole-cell GFP/nuclear-YFP labeling. For the expression of green fluorescent protein (GFP) in cancer cell lines, lentiviral transduction was carried out using the pLex_TRC206-GFP plasmid.

For the expression of nuclear YFP in cancer cell lines, lentiviral transduction was carried out using pmTurquoise2-H2A (Addgene, no. 36207) in which the pmTurquoise was replaced by YFP taken from pQC NLS YFP IX (Addgene, no. 37341).

Drugs. The following drugs were purchased from Sigma Aldrich: DMSO (D2650), doxorubicin (d1515), carboplatin (C2538), gemcitabine (G6423) and irinotecan (I1406). The following drugs were purchased from LC Laboratories: gefitinib (G-4408), trametinib (T-8123), afatinib (A-8644) and 17-AAG (A-6880). The following drugs were purchased from Adooq: lapatinib (A11752), dasatinib (A10290), pemetrexed (A10707), docetaxel (D1000) and 5-FU (A10042).

CTP assessment. On day 0, 6,000 cells per well in 135 µl were plated in 96-well clear-bottom plates (Greiner, no. 60-655090). The next day (day 1), the cells were treated with 15 µl of 10× drug using the CyBi-Well Vario 96/250 Simultaneous Pipettor (CyBio). On day 4, the medium in all wells was manually replaced with 150 µl of fresh medium containing drug treatment. Unless stated otherwise, all cell-imaging was performed using the Operetta automated imaging system (PerkinElmer) at ×2 magnification for whole-cell GFP cells and ×10 magnification for nuclear YFP at days 1 (pre-treatment), 4 and 7 or 8 or 9. Unless stated otherwise, all cell counting was conducted by the Harmony-image analysis tool of the Operetta system. CTP was determined by calculating the quotient of the number of cells after 7–9 d of treatment divided by the number of cells before treatment was initiated (day 1).

Dose-curve/drug-treatment experiments. GFP- or nuclear-YFP-labeled cancer cells at 6,000 cells per well in 135 µl were plated in 96-well clear-bottom plates (Greiner, no. 60-655090). The next day, the cells were treated with 15 µl of 10× drug using the CyBi-Well Vario 96/250 Simultaneous Pipettor (CyBio) either in a single dose or in a dose-curve form. The medium in all wells was manually replaced with fresh medium containing drug treatment every 3–4 d. All experiments were carried out at least in duplicate.

Well-plate experiments. On day 0, nuclear-YFP-labeled PC9 or G361 cancer cells (0.6 cell per well in 10 µl) were plated in 1,536-well clear-bottom plates (Greiner SCREENSTAR, no. 60-789866) with 1:1 ratio of conditioned-medium (see below) and fresh medium containing 20% FCS. After 4–6 h, plates were imaged using the Operetta system to find wells with more than one cell and exclude them from further analysis. After 11–16 d of culture, once clones were large enough, the plate was imaged to count the number of cells per well. Medium was changed using reversed centrifugation and 10 µl per well of drug-containing medium was added by using the CyBi-Well Vario 384/25. The medium in all wells was replaced with fresh medium every 3–4 d. To calculate the CTP of each clone, the number of cells in each well after 7 d of treatment was measured by imaging, as detailed above. For an accurate determination of CTP, we excluded clones with fewer than 240 cells per well before treatment.

CTP-enrichment modeling. To computationally generate a larger population so that its CTP distribution is similar to the CTP distribution of the experimental naive population, each clone was multiplied by 1,000, keeping its CTP value. To simulate drug treatment, we calculated the number of surviving cells and their CTP by multiplying the number of cells in each clone (1,000) by the CTP. Clones CTP values in our model were kept constant and did not change with treatment. A histogram of the CTP of the remaining clones was then plotted next to the experimental results.

Generation of single-cell-derived clones. GFP-labeled cancer cells (0.5 cells per well in 150 µl) were seeded on a Corning 96-well plate (no. 3595). After 6–8 h, wells were manually tested for the existence of single cells in each well. Wells with more than one cell were excluded from further handling. After 2–3 weeks, 43 clones were transferred to larger plates and handled as for the parental cell line.

Bulk RNA-seq and analysis. A total of 2×10^6 cells from each clone were seeded on a 10-cm plate and left to settle overnight. Total RNA from different samples was extracted using the Direct-Zol RNA mini-prep kit (Zymo-Research) according to the manufacturer's protocol. The RNA integrity of all samples was assessed by Bioanalyzer to ensure an RNA integrity number score of at least 9 before proceeding to library preparation. Next, 1 µg of RNA from each sample was taken for preparation of an mRNA TrueSeq library in the INCPM unit (Weizmann Institute of Science), which was then sequenced by Illumina HiSeq 2000 sequencing system in single-end 50 nucleotide reads. The reads were aligned to the genome with TopHat (v.2.0.10) algorithm. Estimation of mRNA abundance

was performed by HTseq-count (v.0.6.1p1) and differential expression analysis was performed with the R package DEseq2 algorithm (v.1.6.3).

Proteome analysis. Proteome analysis was performed as described by Hillman et al.[58] A total of 5×10^6 cells from each clone were seeded on six 15-cm plates and left to settle overnight. One plate from each clone was treated with 0.5 µM gefitinib for 24 h before collection. For collection, all plates were washed once with cold PBS and cells were then collected by scraping on ice into 10 ml cold PBS. Cells were centrifuged in 4 °C for 5 min at 250*g*. Samples were kept at −80 °C until processing. Samples were lysed in 6 M urea and 2 M thiourea in 0.1 M Tris buffer (pH 8.5). Proteins were reduced with 1 mM dithiothreitol and alkylated with 5 mM iodoacetamide followed by overnight in-solution digestion with LysC-trypsin mix (Promega) and sequencing-grade modified trypsin (Promega). The resulting peptides were separated using strong cation exchange fractionation and desalted on C18 stage tips. Samples were analyzed by high-performance liquid chromatography (Easy nLC 1000 HPLC system; Thermo Fisher Scientific) coupled online to a Q-Exactive Plus mass spectrometer (Thermo Fisher Scientific) using the NSI ionization source with spray voltage of 2.10 kV. Peptides from each fraction were separated with a flow rate of 0.3 µl min^{-1} for 140-min linear gradient of water–acetonitrile using a PepMap 50-cm-long C18 column. All measurements were conducted in positive mode.

Raw MS files were analyzed by MaxQuant (v.1.5.3.36) with the integrated Andromeda search engine. MS/MS searches were performed against the human Uniprot database (published September 2015). A false discovery rate cutoff of 1% was applied to both protein and peptide identification. To obtain quantitative data, the label-free quantification algorithm was used.

Antibody arrays. Antibody arrays were purchased from Ray-Biotech (no. AAH-APO-1-2) and used according to the manufacturer's protocol.

Generating single-cell-derived clones for MARS-seq. GFP-labeled cancer cells (0.5 cells per well in 50 µl) were plated on a black clear-bottom 384-well plate (Corning, no. 3712). At 6–8 h after plating, plates were imaged by the Operetta automated imaging system (PerkinElmer) at ×2 magnification and wells containing one cell were selected. Cells were cultured for ~2–3 weeks and clonal populations that have reached to 80–100% confluency by then were moved to Corning 96-well plate (no. 3595). After 48 h clones were split into 6×96-well plates and were cultured for an additional 24 h. Then, two plates were used for measuring $CTP_{gefitinib}$ as described above, two plates were used for measuring the population doubling time as described above and two plates were treated for 24 h with either DMSO or 0.5 µM gefitinib and were then used for MARS-seq.

MARS-seq clone collection. To process each clonal population to transcriptome analysis by MARS-seq, clones were washed with 150 µl PBS (Biological Industries, no. 02-023-1A) and detached by the addition of 30 µl trypsin b (Biological Industries, no. 03-052-1B) for 3 min at 37 °C. Then, 1 µm of Lysis buffer per 50 cells was added. The lysis buffer contained 0.005% RNase inhibitor (RNAsin plus, Promega, no. N2611) and 10% Triton X-100 (Sigma Aldrich, no. 9002-93-1).

MARS-seq multiplexed transcriptional analysis of clonal populations. Lysed clonal population were manually transferred in four replicates of 1 µl into MARS-seq 384-well plates containing 2 µl of barcoded reverse transcription primers (concentration of 8 nM in each well). Downstream library preparation was performed according to Jaitin et al.[59] and by using a randomized unique molecular identifier (UMI) sequence of eight base pairs (allowing a maximal count of ~65,000 UMIs per gene per well). Library preparation was identical to that used for single cells, with the only exception of extending the 95 °C evaporation step before RT1 from 3 min to 4 min, to compensate for the higher volume.

MARS-seq mapping and low-level analysis of single cells and clonal RNA-seq data. Libraries were sequenced by paired end 150-bp sequencing on Nextseq 500 to a mean depth of 374,071 and 348,357 reads per treated and untreated clones, respectively. The 37 bp of read1 were used for mapping (default bowtie2 parameters, hg19 reference genome, 3′ untranslated region (UTR) gene intervals). UMIs from four replicate wells assigned to each PC9 single-cell-derived clone were aggregated, resulting in 212 untreated and 210 treated clonal populations sampled by at least 10,000 UMIs. Some of the downstream analysis was performed on 194 matching pairs of clonal populations that had sufficient coverage both with and without treatment and had a measured CTP value.

Phosphoproteomics. Two very low (~2%), two low (~5–10%), two high (~20–25%) and two very high (~85–90%) CTP clones were profiled by phosphoproteomics, each with three biological replicates. The samples were lysed with 5% SDS in 50 mM Tris-HCl, pH 7.4 and subjected to tryptic digestion using an S-trap, followed by a phosphor-enrichment using immobilized metal (Fe^{+3}) affinity chromatography on a robotic system (Bravo).

Liquid chromatography–mass spectrometry. The resulting peptides were analyzed using nanoflow liquid chromatography (10 kpsi nanoAcquity; Waters). The mobile phase was (A) water + 0.1% formic acid and (B) acetonitrile + 0.1% formic acid. Desalting of the samples was performed online using a reversed-phase Symmetry C18 trapping column (180 µm internal diameter, 20 mm length, 5 µm particle size; Waters). Peptides were separated using a T3 HSS nano-column (75 µm internal diameter, 250 mm length, 1.8 µm particle size; Waters) at 0.35 µl min^{-1}. Peptides were eluted from the column into the mass spectrometer using the following gradient: 4% to 20% B in 155 min, 20% to 90% B in 5 min, maintained at 90% for 5 min and then back to initial conditions. The nanoUPLC was coupled online through a nanoESI emitter (10-µm tip; New Objective) to a quadrupole orbitrap mass spectrometer (Fusion Lumos, Thermo Scientific) using FlexIon nanospray apparatus (Proxeon). Data were acquired in data-dependent acquisition mode. MS1 resolution was set to 120,000 (at 200 m/z), mass range of m/z 375–1,650, AGC of 4×10^5 and maximum injection time was set to 50 ms. MS2 resolution was set to 15,000, AGC of 5×10^4, dynamic exclusion of 30 s and maximum injection time of 150 ms. Each sample was analyzed on the instrument separately in a random order in discovery mode.

Data processing. Raw data were processed with MaxQuant v.1.6.0.16. Data were searched with the Andromeda search engine against the Human proteome database appended with common laboratory protein contaminants and the following modifications: carbamidomethylation of C as a fixed modification and oxidation of M, *N*-terminal acetylation and phosphorylation on S or T or Y as variable. Decoy hits were filtered out, as well as phospho-sites that were identified with localization probability <0.75 and only phospho-sites that had at least two valid values in at least one experimental group were kept. In total, 13,570 phospho-sites were identified and quantified with about 87% enrichment. We excluded three samples (B6_3, B24_1 and SBB5_3) on the basis of the low quality of raw data. Pearson's correlation was calculated on phospho-sites that were detected in all samples with a mean/s.d. value >0.4.

Western blot. Cells were plated a day before treatment on a 10-cm plate at a 1.5×10^6 cells per well and were treated by either DMSO or 0.5 µM gefitinib for 24 h. Cells were then lysed with 100 µl of ice-cold RIPA buffer (Thermo Scientific, Pierce, no. 89901) on ice. Samples were mixed with 4× protein sample-loading buffer (Li-Cor, no. 928-40004) and 10× sample-reducing agent (Li-Cor, no. B0009) and run on a 4–10% Bis-Tris gel at 120 V. Transfer to membranes (Sigma Aldrich, no. 10401380) was performed using Program 2 on the Pierce G2 Fast Blotter (Thermo Fisher Scientific). First, antibodies were used to perform immunoblotting, according to antibody manufacturer specifications. Near-infrared fluorescence was detected with the Odyssey Infrared Imaging System (Li-Cor) and signal intensity was quantified with ImageJ software (v.1.53a). Proteins of interest were normalized to loading-control proteins, GAPDH, tubulin or HSP90. pIGF1R (Tyr1165/1166) was purchased from Santa-cruz (no. sc-135767). Phospho-ERK (Thr202/Tyr204) rabbit monoclonal antibody, pEGFR (Tyr1068) rabbit monoclonal antibody, GAPDH rabbit monoclonal antibody and HSP90 polyclonal antibody were purchased from Cell Signaling (nos. 4370, 3777, 2118 and 4874). β-tubulin mouse monoclonal antibody was purchased from Sigma Aldrich (no. SAB4200715). Anti-mouse secondary antibody and anti-rabbit secondary antibody were purchased from Li-Cor (nos. 926-32211 and 926-68070).

FACS analysis of cell cycle. Floating and adherent cells were collected and fixed overnight in 100% cold methanol. Cells were rehydrated in PBS for 30 min, followed by staining with propidium iodide (25 µg ml^{-1})/RNase A (50 µg ml^{-1}). A BDBiosciences LSR II flow cytometer was used to acquire samples. At least 30,000 cells were acquired per sample. Analysis was conducted using FlowJo v.10.7.1. Single cells were gated according to PI-A/PI-H (Extended Data Fig. 3g). Cell-cycle phases were determined by the cell-cycle module of the FlowJo program based on propidium iodide fluorescence.

Overexpression of human IRS1 and mutant. For overexpression of IRS1, GenScript (no. OHu24973D) human IRS1 expression plasmid and pcDNA3.1+/C-(K)-DYK empty-vector plasmid were used. A construct was also made in which all of the following sites were mutated to alanine: S3, S268, S270, S330, S348, T530, S531, S1078 and S1101 (GeneScript Biotech). Transfection was conducted using JetPrime reagent, according to the manufacturer's protocol. Two PC9 clones (A7 and Q4E12) were transfected with either WT IRS1 or mutant IRS1 in six-well plates (250,000 cells per well). The following day, cells were transferred to 6-cm plates and selected with 800 µg ml^{-1} of G418 for 5 d. Cells were then transferred to 10-cm plates and selection was continued with 400 µg ml^{-1} of G418 until plates were ~90% full. At this time, cells were used for experimentation.

siRNA of IRS1. Dharmacon ON-TARGETplus siIRS1 smart-pool (no. B-002000-UB-100) and Dharmacon siLUC control (no. CTM-505294) were used. Transfection was performed using JetPrime reagent, according to the manufacturer's protocol.

Ex vivo organ culture. Ex vivo organ culture was performed as described by Ben-Hamo et al.[60]. Mouse experiments were performed in accordance with the Institutional Animal Care and Use Committee guidelines. The PDX model was

purchased from the Jackson Laboratory (no. TM00199) by the Weizmann Institute and licensed for institutional use. Mice were killed with CO_2 and tumor tissues were removed and placed in ice-cold PBS. Tumors were cut to 250-µm thick slices using a vibratome (VF300, Precisionary Instruments), placed in six-well plates on titanium grids (Alabama R&D) with 4 ml of DMEM/F12 medium (supplemented with 5% FCS, penicillin 100 IU ml^{-1} with streptomycin 100 µg ml^{-1}, amphotericin B 2.5 µg ml^{-1}, gentamycin sulfate 50 mg ml^{-1} and L-glutamine 100 µl ml^{-1}). Tissue was cultured at 37 °C, 5% CO_2 and 80% O_2 on an orbital shaker (TOU-120N, MRC) at 70 r.p.m. The following day, tissue was treated with drugs as indicated for 96 h and formalin-fixed paraffin embedded after overnight fixation. For human tissues, after resection of tumors, the tissue was directly transported to the pathology department. A small sample of approximately 1 cm^3 was taken and placed in ice-cold PBS for immediate transfer to the laboratory for ex vivo organ culturing. All experiments were performed in accordance with the Sheba Medical Center Ethics Committee's approval (SMC-4744) and after obtaining informed consent. Specimen was coded anonymously before its arrival to the laboratory.

Tissue immunohistochemistry. IHC was performed on 4-µm sections from formalin-fixed paraffin embedded tissue samples from ex vivo organ culture. Hematoxylin and eosin staining was performed using an automated stainer. Anti-pIRS1 ser1101 (LifeSpan BioSciences, no. LS-C352384; 1:100 dilution) was added after deparaffinization, blocking of endogenous peroxide with 3% H_2O_2 and heat-induced epitope antigen retrieval. Human tissue was assessed for viability and pIRS staining by an independent blinded pathologist. All histological samples were scanned using the Pannoramic SCAN II (3DHistech).

Patient data. NSCLC for ex vivo organ culture (Fig. 5g) was obtained from the Sheba Medical Center. Informed consent was obtained. The study was approved by the Sheba Medical Center Institutional Review Board (protocol no. SMC-4744) as well as by the Israeli Ministry of Health Ethics Committee (protocol no. 057-2007).

Mice experiments. *Materials.* NT219 was kindly provided by TyrNovo. For the HNSCC and the NSCLC PDX studies, NT219 was formulated for intravenous (i.v.) administration to mice in 20% 2-hydroxypropyl-β-cyclodextrin solution. Cetuximab (ERBITUX 5 mg ml^{-1}, no. 158863) was purchased from Merck; osimertinib (AZD9291) was kindly donated by the 'Chaverim La'refuah' non-profit organization.

Establishment of PDX models. PDX studies were approved by the Medical Ethics Committee of Ziv Hospital in Zfat and by the Medical Ethics Committee of Rabin Medical Center in Petach Tiqva and the Israeli Ministry of Health. Fragments of fresh biopsies from HNSCC (salivary gland mucoepidermoid carcinoma) and from a NSCLC (a bone marrow metastasis with EGFR exon 19 deletion and T790M mutation) were subcutaneously implanted (passage 0, P0) into the nape area of 6-week-old NOD/SCID mice (Harlan). When the tumor size was 1,200–1,500 mm^3, mice were killed and tumors were dissociated by gentleMACS Octo Dissociator in saline and injected subcutaneously to the nape area of the study mice (7–8-week-old NOD/SCID mice, Bar-Ilan University). All procedures were performed under sterile conditions at the Faculty of Medicine, Bar-Ilan University and carried out in accordance with the Guide for the Care and Use of Laboratory Animals of the National Institutes of Health and approved by the ethics committee of animal experiments of Bar-Ilan University. Assignment of the animals to groups was based on baseline data (tumor volumes on day 0), to attain treatment groups with similar mean tumor volume. Following dosing initiation, animals were checked daily for morbidity and mortality. Tumor dimensions, body weight and clinical signs were recorded at least twice a week. After reaching the maximal tumor burden permitted by the ethics committee (1,500 mm^3), mice were killed within 24 h. Mice were housed at an ambient temperature of 22 °C with a 12-h light–dark cycle in a humidity-controlled (55 ± 10%) environment. Food and water were available ad libitum.

NSCLC study. A PDX model of the osimertinib-resistant NSCLC described above (P1) was used to evaluate the anticancer efficacy of osimertinib with and without NT219. Twenty male mice (8 weeks old, Faculty of Medicine, Bar-Ilan University) with tumor volume of ~110 mm^3 were divided into four groups of five mice per group with similar mean tumor volumes and body weights. The mice were treated for 1 week with either osimertinib (5 mg kg^{-1}, orally five times per week); NT219 (65 mg kg^{-1}, 2.5 ml kg^{-1} i.v., twice a week); the combination of osimertinib and NT219 at the same regimens indicated for each of them alone; and vehicle (20% 2-hydroxypropyl-β-cyclodextrin, 2.5 ml kg^{-1} i.v. twice a week). All groups received an additional treatment on day 15. In this aggressive model two mice in each group were found dead on days 12–17 and the rest were killed on day 17, when the control group mice reached the tumor burden end point.

HNSCC study. The PDX model of HNSCC described above (passage 6), implanted in 7-week-old female NOD/SCID mice (Bar-Ilan University), was used for this study. The study was initiated when tumor volume was ~115 mm^3 and included four treatment groups of 3–4 mice per group with similar tumor volumes and body weights. The mice were treated for 9 d with cetuximab (1 mg per mouse intraperitoneally, on days 0, 4, 6 and 9); NT219 (65 mg kg^{-1} i.v., on days 0, 2, 4, 6 and 9); the combination of cetuximab and NT219 at the same regimens indicated for each of them alone, where NT219 was administered 4 h before cetuximab; or vehicle (sterile water 0.2 ml per mouse orally daily).

Data analysis of mice experiments. The length (l) and the width (w) of the tumors were measured 2–4 times a week and the volumes (v) of the tumors were calculated by $v = lw^2/2$. Descriptive statistics including mean and s.e.m. (reported graphically) were calculated for tumor volume. The statistical analysis considered the ln-transformed results of tumor volumes at the end of the study. ANOVA followed by Tukey–Kramer tests was used to explore the differences between tumor volumes of the different groups in the NSCLC model and the tumor recurrence time in the HNSCC model. Analysis results provided clear evidence of the efficacy of the combination treatment over the control ($P < 0.05$) or cetuximab ($P < 0.01$), respectively.

Clinical implications of CTP distribution. The heterogeneity in CTP across the cell population affects the long-term impact of therapeutics, as the population becomes gradually skewed toward the more-persistent cells. To observe this in a controlled environment we generated numerically a population of 10^3 cells and examined their response to two in silico drugs, A and B. The response of each cell in the population to drug A is captured by its mortality rate λ_A, which quantifies its probability to die per unit time (day). Therefore, its probability to survive at day t is

$$P(t) = e^{(-\lambda_A t)}, \quad (1)$$

and hence its CTP after a week of treatment is

$$\mathrm{CTP} = e^{(-7\lambda_A)}. \quad (2)$$

Extracting λ_A from a normal distribution $N(\mu,\sigma^2)$ with mean $\mu_A = 0.25$ and variance $\sigma_A^2 = 4.9 \times 10^{-3}$, we obtain the CTP distribution for drug A, P(CTP), as is shown in Extended Data Fig. 10a (blue). For the same population under drug B we extract λ_B from a similar distribution, this time setting $\mu_B = 0.36$ and $\sigma_B^2 = 1.69 \times 10^{-2}$, hence obtaining a CTP distribution with a smaller mean, that is higher mortality, but also a larger variance, namely higher levels of heterogeneity (red).

Next we allow the population $N(t)$ to evolve over time under the two drugs, having each individual cell undergo mortality at its individual rate λ_A or λ_B (Extended Data Fig. 10b). Hence, the probability of each specific cell to survive by time t is given by equation (1) with the appropriate λ_A, λ_B. At first drug B outperforms drug A, as indeed, on average, it kills cells at a higher rate ($\mu_B > \mu_A$). However, due to B's higher variance ($\sigma_B^2 > \sigma_A^2$), its long-term effect is dramatically slowed down, as the population becomes dominated by the high CTP cells, resulting in a crossover at day 17. From this point on, drug A becomes more efficient. Examining the effect of both drugs seventh day, a common practice in clinical assessment, would have rendered B superior, overlooking the impact of the CTP heterogeneity.

For an empirical observation, in Extended Data Fig. 10c we show the cell population $N(t)$ versus day as obtained under the effect of doxorubicin (blue) versus trametinib (red). A crossover of the form shown in the numerical Extended Data Fig. 10b is clearly observed, as the initially superior trametinib is, in the long run, outperformed by doxorubicin. Similar results are obtained for cisplatin versus trametinib (Extended Data Fig. 10d).

Statistics and reproducibility. No statistical method was used to predetermine sample size. Randomization was used in the MARS-seq library preparation and in the order of analysis of the phosphoproteomics samples as described in Methods. Blinding was used in assessment of viability and pIRS staining by an independent pathologist as described in Methods. In the phosphoproteomics experiments samples with lower coverage than expected (<7,000 phospho-sites detected) were excluded from the analysis.

Reporting Summary. Further information on research design is available in the Nature Research Reporting Summary linked to this article.

Data availability

Mass spectrometry phosphoproteomics data have been deposited to the ProteomeXchange Consortium via the PRIDE[61] partner repository with the dataset identifiers PXD026824, PXD026842, PXD026844, PXD026857 and PXD026805. Mass spectrometry proteomics data have been deposited to the ProteomeXchange Consortium via the PRIDE[61] partner repository with the dataset identifier PXD026834. RNA-seq data that support the findings of this study have been deposited in the Gene Expression Omnibus under accession codes GSE178978 and GSE179240. Source data are provided with this paper.

Code availability

Code for Extended Data Fig. 10 is found at https://doi.org/10.5281/zenodo.5036166.

Received: 13 March 2020; Accepted: 23 August 2021;
Published online: 21 October 2021

References

1. Gupta, P. B. et al. Stochastic state transitions give rise to phenotypic equilibrium in populations of cancer cells. *Cell* **146**, 633–644 (2011).
2. Chaffer, C. L. et al. Normal and neoplastic nonstem cells can spontaneously convert to a stem-like state. *Proc. Natl Acad. Sci. USA* **108**, 7950–7955 (2011).
3. Lamouille, S., Xu, J. & Derynck, R. Molecular mechanisms of epithelial–mesenchymal transition. *Nat. Rev. Mol. Cell Biol.* **15**, 178–196 (2014).
4. Knoechel, B. et al. An epigenetic mechanism of resistance to targeted therapy in T cell acute lymphoblastic leukemia. *Nat. Genet.* **46**, 364–370 (2014).
5. Lee, M.-C. W. et al. Single-cell analyses of transcriptional heterogeneity during drug tolerance transition in cancer cells by RNA sequencing. *Proc. Natl Acad. Sci. USA* **111**, E4726–E4735 (2014).
6. Sharma, S. V. et al. A chromatin-mediated reversible drug-tolerant state in cancer cell subpopulations. *Cell* **141**, 69–80 (2010).
7. Fallahi-Sichani, M., Honarnejad, S., Heiser, L. M., Gray, J. W. & Sorger, P. K. Metrics other than potency reveal systematic variation in responses to cancer drugs. *Nat. Chem. Biol.* **9**, 708–714 (2013).
8. Balaban, N. Q., Merrin, J., Chait, R., Kowalik, L. & Leibler, S. Bacterial persistence as a phenotypic switch. *Science* **305**, 1622–1625 (2004).
9. Bigger, J. Treatment of staphylococcal infections with penicillin by intermittent sterilisation. *Lancet* **244**, 497–500 (1944).
10. Hata, A. N. et al. Tumor cells can follow distinct evolutionary paths to become resistant to epidermal growth factor receptor inhibition. *Nat. Med.* https://doi.org/10.1038/nm.4040 (2016).
11. Liao, B.-C., Lin, C.-C. & Yang, J. C.-H. Second and third-generation epidermal growth factor receptor tyrosine kinase inhibitors in advanced nonsmall cell lung cancer. *Curr. Opin. Oncol.* **27**, 94–101 (2015).
12. Pao, W. et al. Acquired resistance of lung adenocarcinomas to gefitinib or erlotinib is associated with a second mutation in the EGFR kinase domain. *PLoS Med.* **2**, e73 (2005).
13. Fridman, O., Goldberg, A., Ronin, I., Shoresh, N. & Balaban, N. Q. Optimization of lag time underlies antibiotic tolerance in evolved bacterial populations. *Nature* **513**, 418–421 (2014).
14. Pearl Mizrahi, S., Gefen, O., Simon, I. & Balaban, N. Q. Persistence to anti-cancer treatments in the stationary to proliferating transition. *Cell Cycle* https://doi.org/10.1080/15384101.2016.1248006 (2016).
15. Hangauer, M. J. et al. Drug-tolerant persister cancer cells are vulnerable to GPX4 inhibition. *Nature* **551**, 247–250 (2017).
16. Terai, H. et al. ER stress signaling promotes the survival of cancer 'persister cells' tolerant to EGFR tyrosine kinase inhibitors. *Cancer Res.* https://doi.org/10.1158/0008-5472.CAN-17-1904 (2017).
17. Tetsu, O., Phuchareon, J., Eisele, D. W., Hangauer, M. J. & McCormick, F. AKT inactivation causes persistent drug tolerance to EGFR inhibitors. *Pharmacol. Res.* **102**, 132–137 (2015).
18. Raha, D. et al. The cancer stem cell marker aldehyde dehydrogenase is required to maintain a drug-tolerant tumor cell subpopulation. *Cancer Res.* https://doi.org/10.1158/0008-5472.CAN-13-3456 (2014).
19. Shaffer, S. M. et al. Rare cell variability and drug-induced reprogramming as a mode of cancer drug resistance. *Nature* https://doi.org/10.1038/nature22794 (2017).
20. Kokubo, Y. et al. Reduction of PTEN protein and loss of epidermal growth factor receptor gene mutation in lung cancer with natural resistance to gefitinib (IRESSA). *Br. J. Cancer* **92**, 1711–1719 (2005).
21. Raoof, S. et al. Targeting FGFR overcomes EMT-mediated resistance in EGFR mutant non-small cell lung cancer. *Oncogene* https://doi.org/10.1038/s41388-019-0887-2 (2019).
22. Shah, K. N. et al. Aurora kinase A drives the evolution of resistance to third generation EGFR inhibitors in lung cancer. *Nat. Med.* **25**, 111–118 (2019).
23. Wakata, K. et al. A favourable prognostic marker for EGFR mutant non-small cell lung cancer: immunohistochemical analysis of MUC5B. *BMJ Open* **5**, e008366 (2015).
24. Corominas-Faja, B. et al. Stem cell-like ALDH(bright) cellular states in EGFR-mutant non-small cell lung cancer: a novel mechanism of acquired resistance to erlotinib targetable with the natural polyphenol silibinin. *Cell Cycle* **12**, 3390–3404 (2013).
25. Shaw, L. M. The insulin receptor substrate (IRS) proteins: at the intersection of metabolism and cancer. *Cell Cycle* **10**, 1750–1756 (2011).
26. Copps, K. D. & White, M. F. Regulation of insulin sensitivity by serine/threonine phosphorylation of insulin receptor substrate proteins IRS1 and IRS2. *Diabetologia* **55**, 2565–2582 (2012).
27. Li, L. et al. Acquisition of EGFR TKI resistance and EMT phenotype is linked with activation of IGF1R/NF-κB pathway in EGFR-mutant NSCLC. *Oncotarget* **8**, 92240–92253 (2017).
28. Cassell, A. & Grandis, J. R. Investigational EGFR-targeted therapies in HNSCC. *Expert Opin. Investig. Drugs* **19**, 709–722 (2010).
29. Grandis, J. R. & Tweardy, D. J. Elevated levels of transforming growth factor α and epidermal growth factor receptor messenger RNA are early markers of carcinogenesis in head and neck cancer. *Cancer Res.* **53**, 3579–3584 (1993).
30. Ozanne, B., Richards, C. S., Hendler, F., Burns, D. & Gusterson, B. Over-expression of the EGF receptor is a hallmark of squamous cell carcinomas. *J. Pathol.* **149**, 9–14 (1986).
31. Kanety, H., Feinstein, R., Papa, M. Z., Hemi, R. & Karasik, A. Tumor necrosis factor α-induced phosphorylation of insulin receptor substrate-1 (IRS-1). Possible mechanism for suppression of insulin-stimulated tyrosine phosphorylation of IRS-1. *J. Biol. Chem.* **270**, 23780–23784 (1995).
32. El-Ami, T. et al. A novel inhibitor of the insulin/IGF signaling pathway protects from age-onset, neurodegeneration-linked proteotoxicity. *Aging Cell* **13**, 165–174 (2014).
33. Ibuki, N. et al. The tyrphostin NT157 suppresses insulin receptor substrates and augments therapeutic response of prostate cancer. *Mol. Cancer Ther.* **13**, 2827–2839 (2014).
34. Reuveni, H. et al. Therapeutic destruction of insulin receptor substrates for cancer treatment. *Cancer Res.* **73**, 4383–4394 (2013).
35. Ramirez, M. et al. Diverse drug-resistance mechanisms can emerge from drug-tolerant cancer persister cells. *Nat. Commun.* **7**, 10690 (2016).
36. Russo, M. et al. Adaptive mutability of colorectal cancers in response to targeted therapies. *Science* https://doi.org/10.1126/science.aav4474 (2019).
37. Banelli, B. et al. The histone demethylase KDM5A is a key factor for the resistance to temozolomide in glioblastoma. *Cell Cycle* **14**, 3418–3429 (2015).
38. Murakami, A. et al. Hypoxia increases gefitinib-resistant lung cancer stem cells through the activation of insulin-like growth factor 1 receptor. *PLoS ONE* **9**, e86459 (2014).
39. Vinogradova, M. et al. An inhibitor of KDM5 demethylases reduces survival of drug-tolerant cancer cells. *Nat. Chem. Biol.* **12**, 531–538 (2016).
40. Viswanathan, V. S. et al. Dependency of a therapy-resistant state of cancer cells on a lipid peroxidase pathway. *Nature* **547**, 453–457 (2017).
41. Guler, G. D. et al. Repression of stress-induced LINE-1 expression protects cancer cell subpopulations from lethal drug exposure. *Cancer Cell* https://doi.org/10.1016/j.ccell.2017.07.002 (2017).
42. Shaffer, S. M. et al. Memory sequencing reveals heritable single-cell gene expression programs associated with distinct cellular behaviors. *Cell* **182**, 947–959.e17 (2020).
43. Spencer, S. L., Gaudet, S., Albeck, J. G., Burke, J. M. & Sorger, P. K. Non-genetic origins of cell-to-cell variability in TRAIL-induced apoptosis. *Nature* **459**, 428–432 (2009).
44. Faber, A. C. et al. BIM expression in treatment-naive cancers predicts responsiveness to kinase inhibitors. *Cancer Discov.* **1**, 352–365 (2011).
45. Faber, A. C. et al. Epithelial-to-mesenchymal transition antagonizes response to targeted therapies in lung cancer by suppressing BIM. *Clin. Cancer Res.* https://doi.org/10.1158/1078-0432.CCR-17-1577 (2017).
46. Song, K.-A. et al. Epithelial-to-mesenchymal transition antagonizes response to targeted therapies in lung cancer by suppressing BIM. *Clin. Cancer Res.* **24**, 197–208 (2018).
47. Rehman, S. K. et al. Colorectal cancer cells enter a diapause-like DTP state to survive chemotherapy. *Cell* **184**, 226–242 (2021).
48. Zhang, Y. Persisters, persistent infections and the yin–yang model. *Emerg. Microbes Infect.* **3**, e3 (2014).
49. Raj, A. & Oudenaarden, Avan Nature, nurture, or chance: stochastic gene expression and its consequences. *Cell* **135**, 216–226 (2008).
50. Barria, A., Muller, D., Derkach, V., Griffith, L. C. & Soderling, T. R. Regulatory phosphorylation of AMPA-type glutamate receptors by CaM-KII during long-term potentiation. *Science* **276**, 2042–2045 (1997).
51. Lee, H. K., Barbarosie, M., Kameyama, K., Bear, M. F. & Huganir, R. L. Regulation of distinct AMPA receptor phosphorylation sites during bidirectional synaptic plasticity. *Nature* **405**, 955–959 (2000).
52. Sweatt, J. D. Memory mechanisms: the yin and yang of protein phosphorylation. *Curr. Biol.* **11**, R391–R394 (2001).
53. Langlais, P. et al. Global IRS-1 phosphorylation analysis in insulin resistance. *Diabetologia* **54**, 2878–2889 (2011).
54. Yarchoan, M. et al. Abnormal serine phosphorylation of insulin receptor substrate 1 is associated with tau pathology in Alzheimer's disease and tauopathies. *Acta Neuropathol.* **128**, 679–689 (2014).
55. Wang, W. et al. Serine phosphorylation of IRS1 correlates with Aβ-unrelated memory deficits and elevation in Aβ level prior to the onset of memory decline in AD. *Nutrients* https://doi.org/10.3390/nu11081942 (2019).
56. Prasetyanti, P. R. & Medema, J. P. Intra-tumor heterogeneity from a cancer stem cell perspective. *Mol. Cancer* **16**, 1476–4598 (2017).
57. Rios, A. C. et al. Intraclonal plasticity in mammary tumors revealed through large-scale single-cell resolution 3D imaging. *Cancer Cell* **35**, 618–632 (2019).
58. Hillman, Y. et al. MicroRNAs affect complement regulator expression and mitochondrial activity to modulate cell resistance to complement-dependent cytotoxicity. *Cancer Immunol. Res.* https://doi.org/10.1158/2326-6066.CIR-18-0818 (2019).

59. Jaitin, D. A. et al. Massively parallel single-cell RNA-seq for marker-free decomposition of tissues into cell types. *Science* **343**, 776–779 (2014).
60. Ben-Hamo, R. et al. Predicting and affecting response to cancer therapy based on pathway-level biomarkers. *Nat. Commun*. https://doi.org/10.1038/s41467-020-17090-y (2020).
61. Perez-Riverol, Y. et al. The PRIDE database and related tools and resources in 2019: improving support for quantification data. *Nucleic Acids Res.* **47**, D442–D450 (2019).

Acknowledgements

We thank D. Douek, I. Ben-Porath and O. Sandler for their comments. We thank Champions Oncology for providing HNSCC patient tumor microarrays and PDX data. We thank M. Berger for assistance with the preparation of the figures. R.S. was partially funded by the Fabrikant-Morse Families Research Fund for Humanity, the Moross Integrated Cancer Center and the Rising Tide Foundation. R.S. is the incumbent of the Roel C. Buck Career Development Chair. I.H. was partially funded by Leona M. and Harry B. Helmsley Charitable Trust grant no. 2012PG-ISL013. I.H. and S.M.S. were partially funded by the Rabin Medical Center–Bar-Ilan grant project. G.F. is the incumbent of the David and Stacey Cynamon Research fellow Chair in Genetics and Personalized Medicine.

Author contributions

Conceptualization was provided by A.J.B. and R.S. Experimental design and performance was conducted by A.J.B., E.G., Z.M., N.G., Y.Z., A.P., S.G., H.R., L.K., G.B., E.M., S.M.S., M.M., Y.R., J.B., I.K. and R.S. Data analysis was performed by A.J.B., E.G., Z.M., I.H., Y.R., G.F., T.G., Y.L., A.T., H.R. and R.S. Modeling was conducted by S.K.S. and Y.P. Mathematical analysis was performed by U.H. and B.B. A.J.B. and R.S. were responsible for writing the original draft of the manuscript. Supervision was carried out by R.S.

Competing interests

R.S. and N.G. serve as external consultants to CuResponse, a company that utilizes ex vivo organ culture technology and have been issued equity incentives in the company. H.R. and L.K. are employees of TyrNovo, a company that develops NT219 as a potential anticancer agent, are co-inventors on NT219 patent/patent applications and have been issued equity incentives in the company. I.H. and S.M.S. are consultants of TyrNovo and have been issued equity incentives in the company.

Additional information

Extended data is available for this paper at https://doi.org/10.1038/s43018-021-00261-1.

Supplementary information The online version contains supplementary material available at https://doi.org/10.1038/s43018-021-00261-1.

Correspondence and requests for materials should be addressed to Ravid Straussman.

Peer review information *Nature Cancer* thanks Yoosik Kim and the other, anonymous, reviewer(s) for their contribution to the peer review of this work.

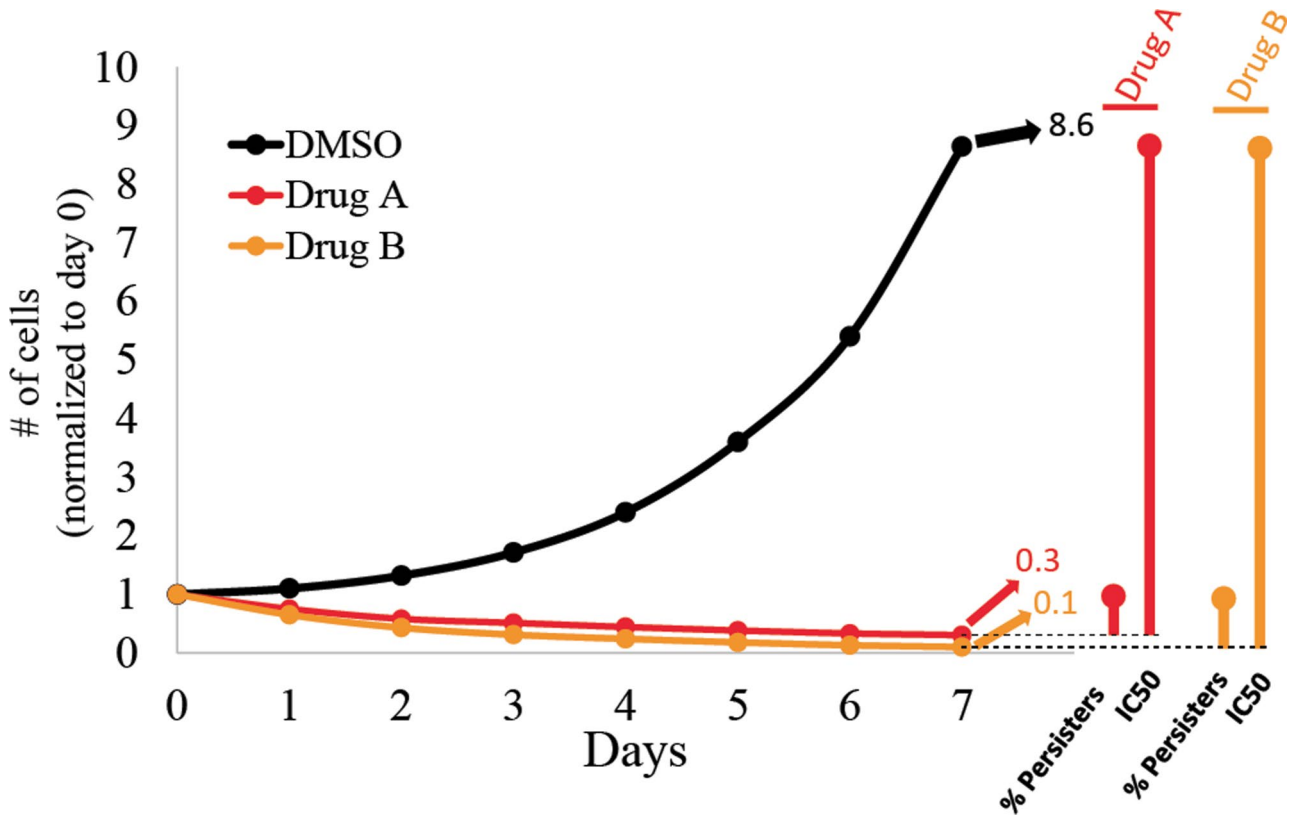

Extended Data Fig. 1 | The relationship between IC50 and frequency of persisters. The graph presents hypothetical data to demonstrate one of the differences between IC50 and frequency of persisters: the different reference point that is used to calculate these measures. IC50 is calculated by comparing the number of cells that remain viable after treatment to the number of cells in the non-treated control. The IC50 thus represents the effect of the drug on both growth rate and cell death. As opposed to IC50, the frequency of persisters is measured by comparing the number of cells that remain viable after treatment to the number of cells that were present just before drug treatment was started. By doing so, we ignore the growth inhibition effect and focus on the cell death effect.

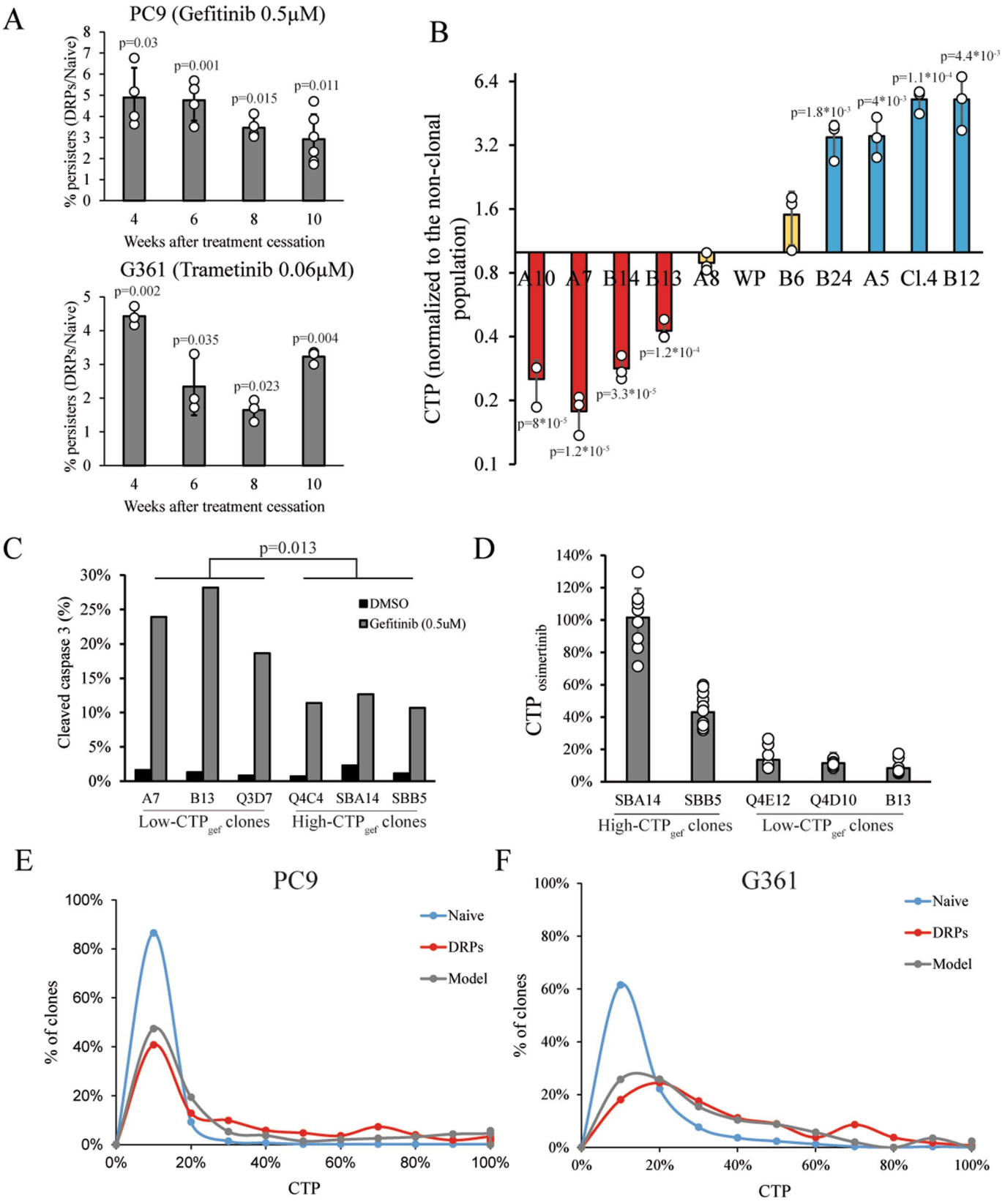

Extended Data Fig. 2 | See next page for caption.

Extended Data Fig. 2 | DRPs have higher percentages of persisters than drug-naive population. (a) The ratio of percent of persisters between PC9 DRPs that were generated by 9 days of gefitinib treatment and then been on drug holiday for 4–10 weeks and PC9 naïve cells is presented for two cell lines treated with the indicated drugs. Data are presented as mean values, bars represent the standard deviation of n = 4 independent cultures for PC9 or n = 3 independent cultures for G361. P-values were obtained by two tailed Student's t-test. **(b)** The $CTP_{gefitinib}$ of the naïve PC9 population and selected 10 of its sub-clones as measured after 9 days of treatment. CTP of the sub-clones was normalized to the CTP of the naïve PC9 non-clonal population. Data are presented as mean values, error bars represent the standard deviation of n = 3 independent cultures. P-values were obtained by two tailed Student's t-test. **(c)** PC9 clones were seeded on day 0 at 1*10^6 cells per 10 cm plate. Gefitinib or DMSO were added on day 1 at 500 nM. Floating and adherent cells were collected 48 h later, fixed and stained with anti cleaved-CASP3 (SCT #9664) followed by anti-rabbit alexa647 secondary antibody, according to the antibody manufacturer commended protocol. Flow cytometry data was acquired and analyzed by CytoFLEX LX. P-value was calculated by two tailed Student's t-test. **(d)** The $CTP_{osimertinib}$ of PC9 clones with known high or low $CTP_{gefitinib}$ was measured after 7 days of treatment. CTP was normalized to the number of cells just before the initiation of treatment. Data are presented as mean values, error bars represent the standard deviation of n = 2 independent cultures. **(e,f)** Histograms of the CTP distribution of PC9 **(e)** and G361 **(f)** cell lines are presented for both the drug-naïve populations (blue) as well as for DRPs of these cell lines (red). CTP of clones was measured after 7 days of treatment with gefitinib. To generate DRP clones, single cells that survived 9 days of gefitinib treatment were let to proliferate into clones without drug. A right shift in the distribution is demonstrated for the DRPs. Modeling of the expected distribution by pure selection of clones according to their CTP is demonstrated in grey.

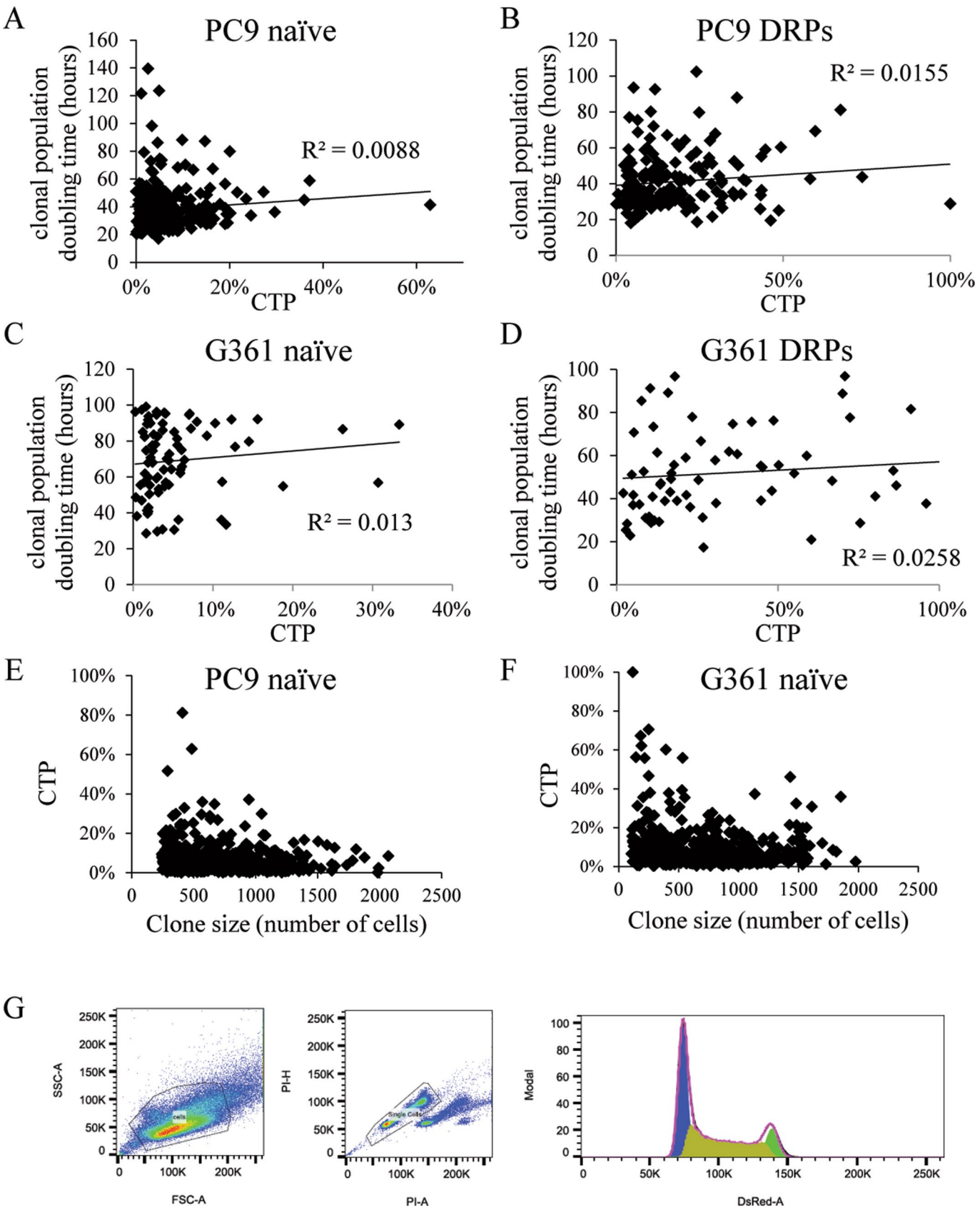

Extended Data Fig. 3 | See next page for caption.

Extended Data Fig. 3 | CTP does not correlate with clonal population doubling time. Scatter plot demonstrating the CTP and clonal population doubling time of 281 naive PC9 clones **(a)** n = 164 PC9 DRPs **(b)** n = 80 naive G361 clones **(c)**, and n = 65 G361 DRPs **(d)**. Single cells from both cell lines were plated on 1536-well plates and left to grow for 11–16 days. To calculate the clonal population doubling time, we counted the number of cells in each well by microscopy at different time points. CTP was measured after 7 days of treatment. Due to short measurement time (24 hours), we excluded clones with PDT > 100 hours from the analysis. **(e,f)** Scatter plot demonstrating the CTP after 7 days of treatment and clone size before treatment for PC9 clones (n = 544 clones) **(e)** and G361 clones (n = 459 clones) **(f). (g)** Gating scheme demonstrating the measurements taken to obtain the cell-cycle distribution presented in Fig. 3f.

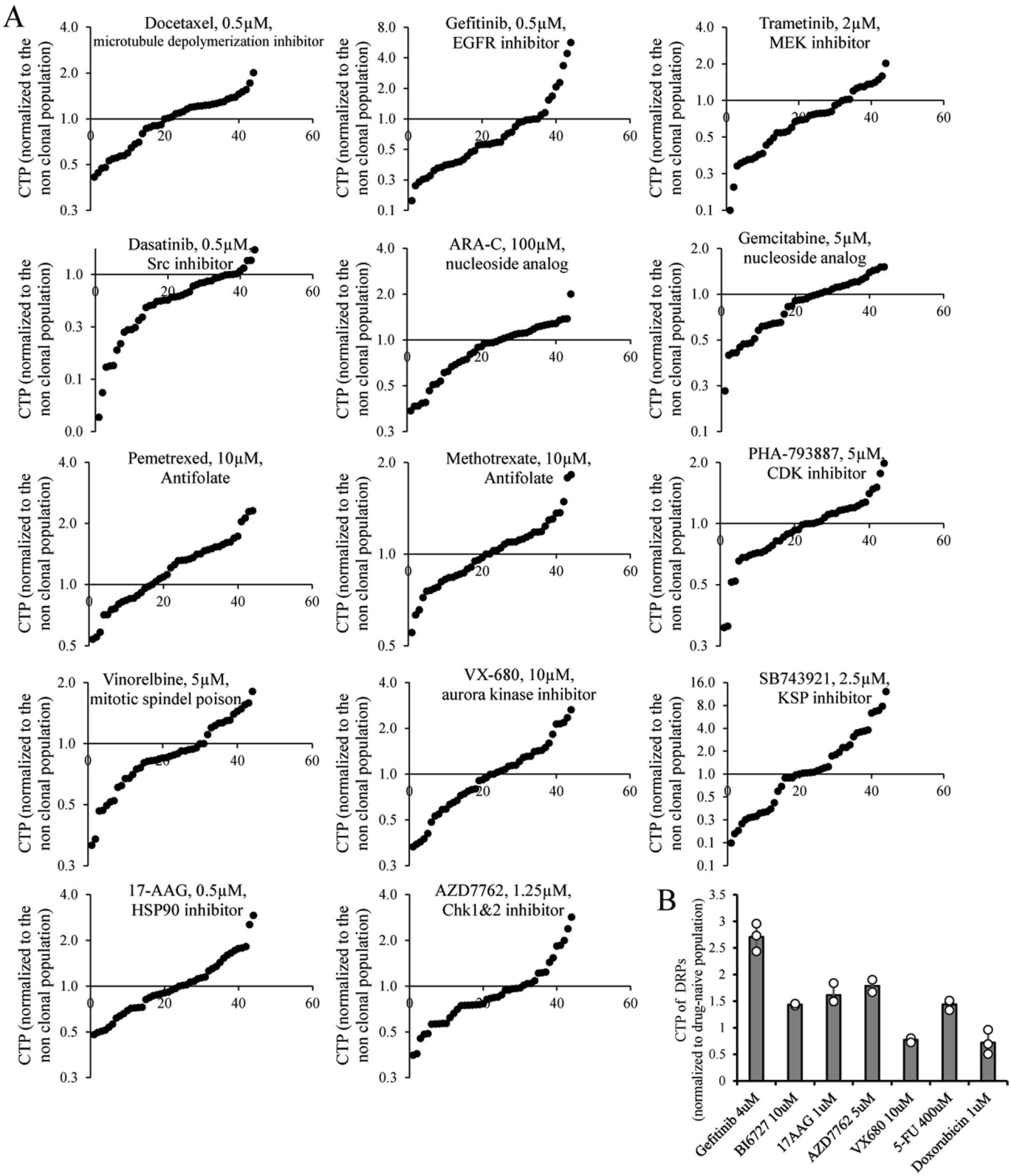

Extended Data Fig. 4 | A wide range of CTPs exist with respect to many drugs. (a) Single-cell derived clones of PC9 (n = 43 clones) as well as the non-clonal population were treated with the indicated drugs and concentrations for 7 days. CTP of each clone was normalized to the CTP of the non-clonal population. For each of the drugs, the clones are ordered based on their CTP **(b)** CTP of HCC2935 DRPs normalized to HCC2935 drug-naïve cells was measured with respect to 7 anti-cancer drugs after 7 days of treatment. HCC2935 DRPs were generated by 0.5uM gefitinib treatment for 11 days followed by drug holiday for 2–3 weeks until cells regained their normal proliferation rate. Error bars represent the standard deviation of n = 3 independent cultures.

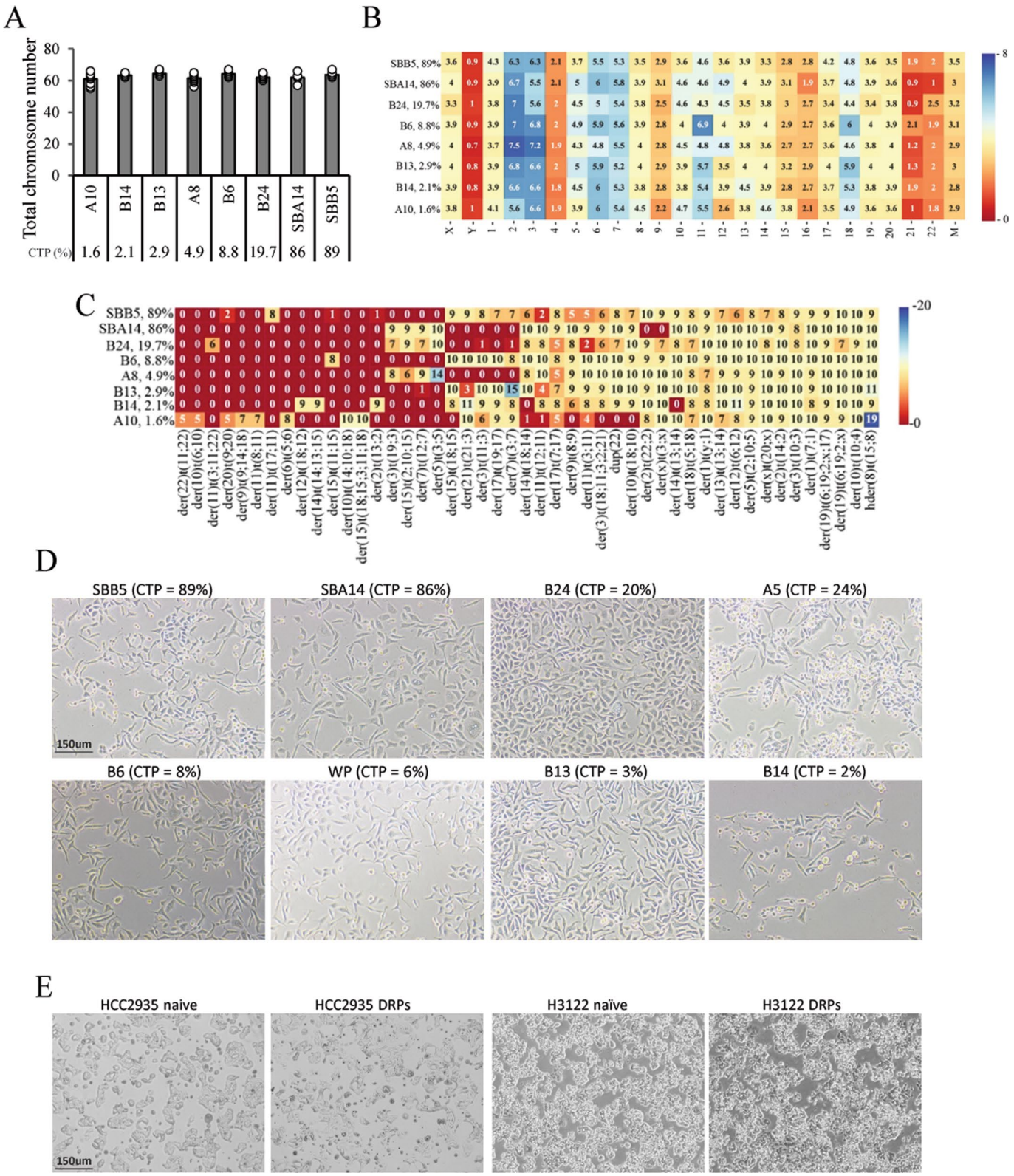

Extended Data Fig. 5 | See next page for caption.

Extended Data Fig. 5 | CTP does not correlate with clonal karyotype changes or specific clonal morphology. (a) Clonal CTP does not correlate with the total number of chromosomes. The average number of chromosomes per PC9 clone was calculated based on karyotype profiling of 10 cells/clone. Chromosomes with translocations were counted as belonging to the main chromosome that constitutes the new chromosomal derivative. Data are presented as mean values, error bars represent standard deviation of n = 10 independent cultures **(b)** Clonal CTP does not correlate to the individual number of chromosomes in each clone. The average number of chromosomes per PC9 clone was calculated based on karyotype profiling of 10 cells/clone. **(c)** Clonal CTP does not correlate with specific chromosomal derivatives (der). The average number of chromosomal aberrations per clone was calculated based on karyotype profiling of 10 cells/clone. **(d)** Representative images of selected PC9 clones with a wide range of $CTP_{Gefitinib}$ (measured after 7 days of treatment) that underwent expansion to generate cell lines are presented. **(e)** Representative images of drug-naïve cells and DRPs of HCC2935 and H3122 cell lines. HCC2935 DRPs were generated by 0.5uM gefitinib treatment for 11 days and H3122 DRPs were generated by 0.5uM crizotinib treatment for 9 days followed by drug holiday for 2–3 weeks until cells regained their normal proliferation rate.

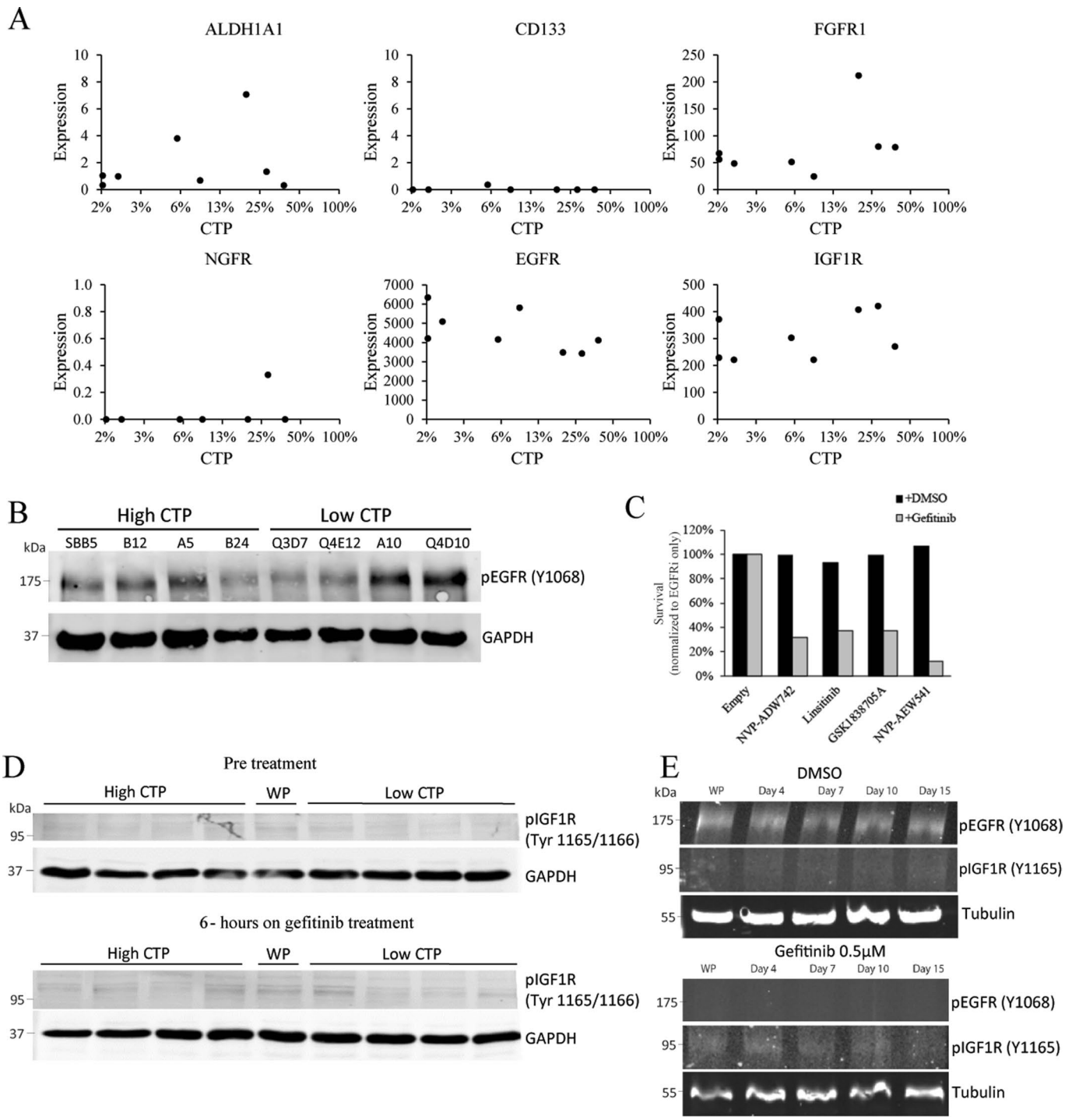

Extended Data Fig. 6 | CTP does not correlate with pIGF1R, pEGFR or the expression of other proteins that were reported to be enriched in persisters. **(a)** A scatter plot demonstrating the correlation between $CTP_{gefitinib}$ after 7 treatment days and averaged expression of genes that were previously suggested to be enriched in persisters. Correlation was tested across seven PC9 clones as well as the non clonal population. Each clone was sequenced in n = 3 independent cultures. **(b)** Levels of phosphor-EGFR were analyzed by western blot in high and low CTP clones (representative blot of n = 2 independent cultures is demonstrated). **(c)** Non-clonal PC9 population was subjected to combination treatment of four IGF1R inhibitors or DMSO control, with or without 1 μM gefitinib. Survival of each combination was normalized to the survival of single treatment with DMSO or gefitinib. **(d)** Protein levels of phosphor-IGF1-R were assayed by western blot analysis pre (upper panel) and 6 hours after (lower panel) treatment with 0.5 μM gefitinib (representative blot of n = 3 independent cultures is demonstrated). **(e)** Protein levels of phospho-EGFR and phospho-IGF1R were assayed by western blot analysis in PC9 drug-naïve cells or PC9 DRPs treated with 0.5uM gefitinib or DMSO control for 24 hours (representative blot of n = 2 independent cultures is demonstrated). To prepare the DRPs, PC9 drug-naïve cells were treated for 4 to 15 days with 0.5uM gefitinib, and then released from drug for additional 2–3 weeks until cells regained their normal proliferation rate.

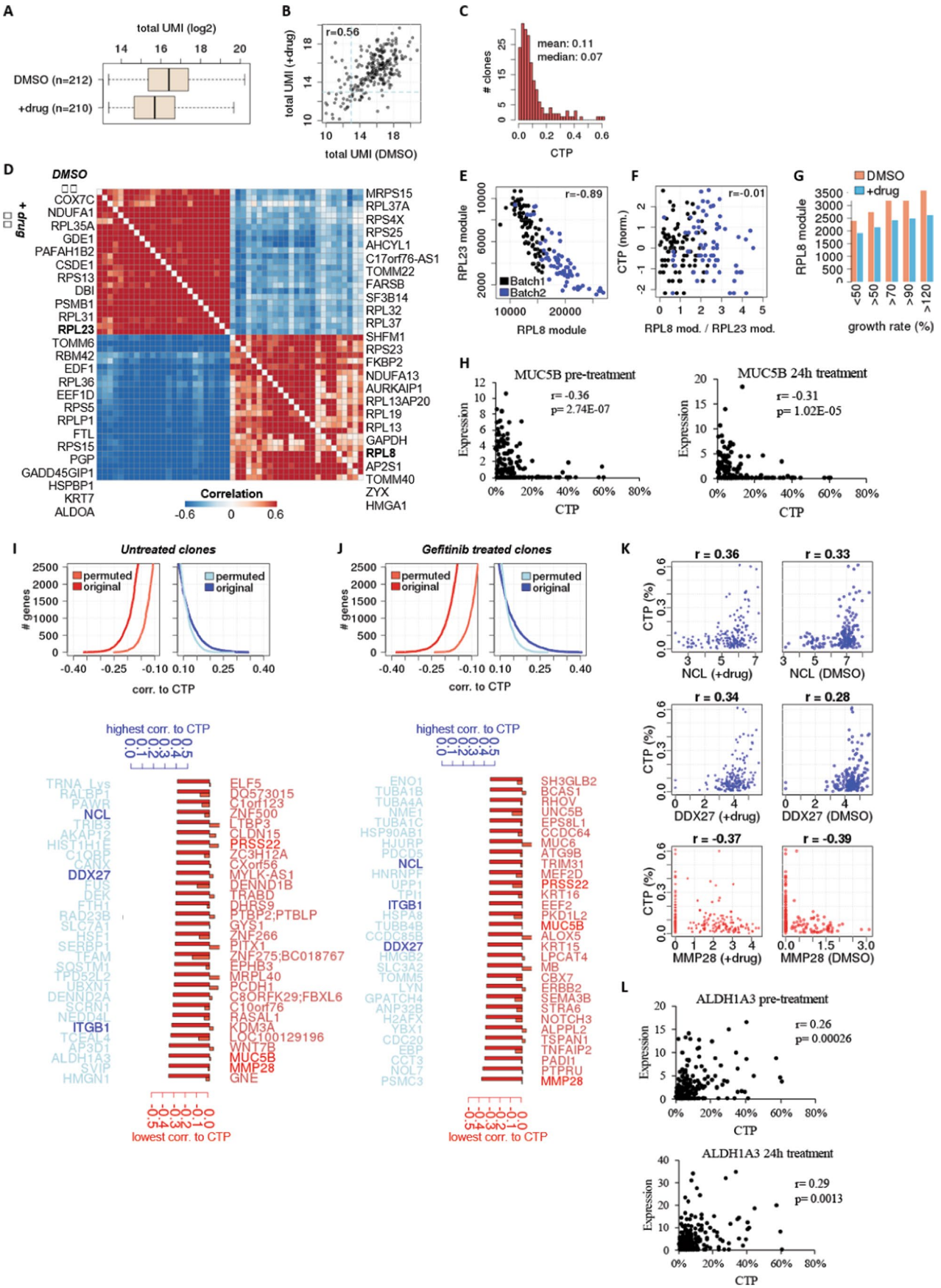

Extended Data Fig. 7 | See next page for caption.

Extended Data Fig. 7 | Transcriptome and CTP analysis in RNAseq of PC9 single cell derived clones. (a) Distributions of total molecules (UMIs) per clone without drug treatment (DMSO) and with gefitinib drug treatment (+drug). Box plots show medians as central lines. Edges of each box represent the interquartile range (IQR) and whiskers mark either 1.5 × IQR or minima/maxima (if no point exceeded 1.5 * IQR). No removal of outliers was performed in this plot. **(b)** log2 of total UMIs obtained per clone in both DMSO (x axis) and drug treatment (y axis). n = 195 single-cell derived clonal populations were sampled by at least 10 K UMIs in both treatments. **(c)** Distribution of clonal CTP values, as measured for n = 195 clones covered in both treatments. **(d)** gene-gene correlation matrix, showing anti-correlation of two proliferation associated gene modules both in DMSO treated clones (upper triangle) and drug treated clones (lower triangle). **(e)** Total normalized expression per clone (UMIs per 100 K UMIs) summed from 200 top correlated genes to RPL8 (x axis) and RPL23 (y axis). Color of dots indicates two culturing batches of clones. **(f)** Expression score per clones for gene modules described in D, computed as log2 ratio of RPL8 / RPL23 total expression (x axis), and is not associated with clonal CTP (y axis). Normalized CTP per clone was computed as log2 ratio of each clone's CTP to median CTP of the relevant culturing batch. **(g)** Expression of RPL8 gene module is positively correlated with growth rates. Clones are binned according to the percentage of increment in cells, measured between 5 and 7 days since splitting cells to growth assay (see Methods), and RPL8 module expression is computed as summation of clonal UMIs for 10 genes with highest correlation to RPL8 (units of UMIs per 100 K UMIs). **(h)** Scatter plots showing the normalized expression of Mucin5B pre- and 24 hours post- 0.5 μM gefitinib treatment. Spearman's correlation coefficient is indicated for each plot. **(i)** Cumulative distributions of Spearman's correlation of individual gene expression to CTP in DMSO treated clones. (Top-left) Showing lowest correlation values obtained between genes and CTP (red), and lowest correlation between genes and a randomized vector of CTP values (orange). (Top-right) Showing highest correlation between genes and CTP (blue), and between genes and a randomized vector of CTP values (lightblue). (Bottom panel) Displaying genes with highest (blue) and lowest (red) correlation to CTP, along with their correlation to randomized CTP vector (lightblue and orange bars). **(j)** as h, for gefitinib treated clones. Highlighting genes that maintain strong correlation to CTP in both drug treated and untreated clones. **(k)** Scatter plots showing log normalized expression of selected genes (x axis) and clonal CTP (y axis). **(l)** Scatter plots showing the normalized expression of ALDH1A3 pre- and 24 hours post- 0.5 μM gefitinib treatment. Spearman's correlation coefficient is indicated for each plot. Statistical significance for H and L was assessed using a two-tailed Student's t-test.

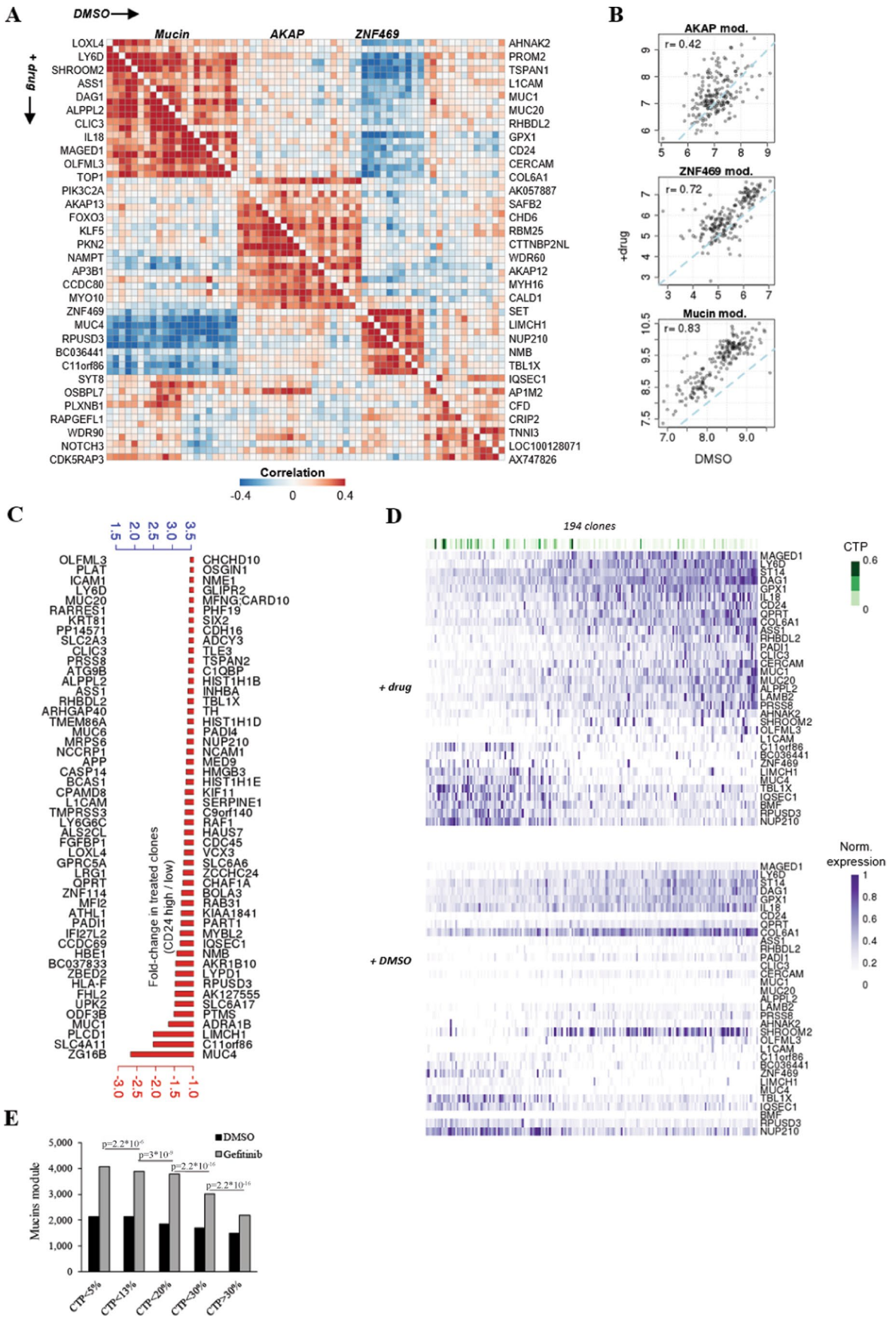

Extended Data Fig. 8 | See next page for caption.

Extended Data Fig. 8 | Gene modules and CTP analysis in RNAseq of PC9 single-cell derived clones. (a) gene-gene correlation matrix, showing gene modules unrelated to proliferation gradient defined in Fig.S7d-g, computed based on normalized expression in untreated clones (upper triangle) and in gefitinib treated clones (lower triangle). **(b)** log normalized clonal expression of gene modules specified in A in untreated (x axis) and drug treated clones (y axis). Dashed light blue line defining the diagonal, indicating changes of absolute expression levels in untreated and treated clones. A higher correlation suggests higher clonal stability of the gene module, amid the transcriptional response to the drug treatment. **(c)** Showing 50 genes with highest (blue) and lowest (red) fold-change in Mucin-high clones vs Mucin-low clones. Fold-change computed as log ratio of expression geometric mean of each gene in 30% of gefitinib treated clones with highest Mucin expression, to its expression geometric mean in 30% of gefitinib treated clones with lowest Mucin expression. **(d)** Clonal expression of Mucin gene module is associated with CTP. Showing expression of genes associated with the Mucin and ZNF469 genes modules shown in A for gefitinib treated (upper panel) and DMSO treated clones (lower panel). Each column in both panel defines clone from the same single-cell-derived clonal population, after eliminating one of the n=195 clones whose CTP-assay failed technically. Expression of each gene is normalized to maximal expression in gefitinib treated clones. Despite the weaker expression in untreated clones, the conserved expression structure which correlated to CTP can be observed also without treatment. **(e)** Average of the mucin gene module score is presented for clones that were grouped by their CTP gefitinib. P-values were calculated using the chi-square test.

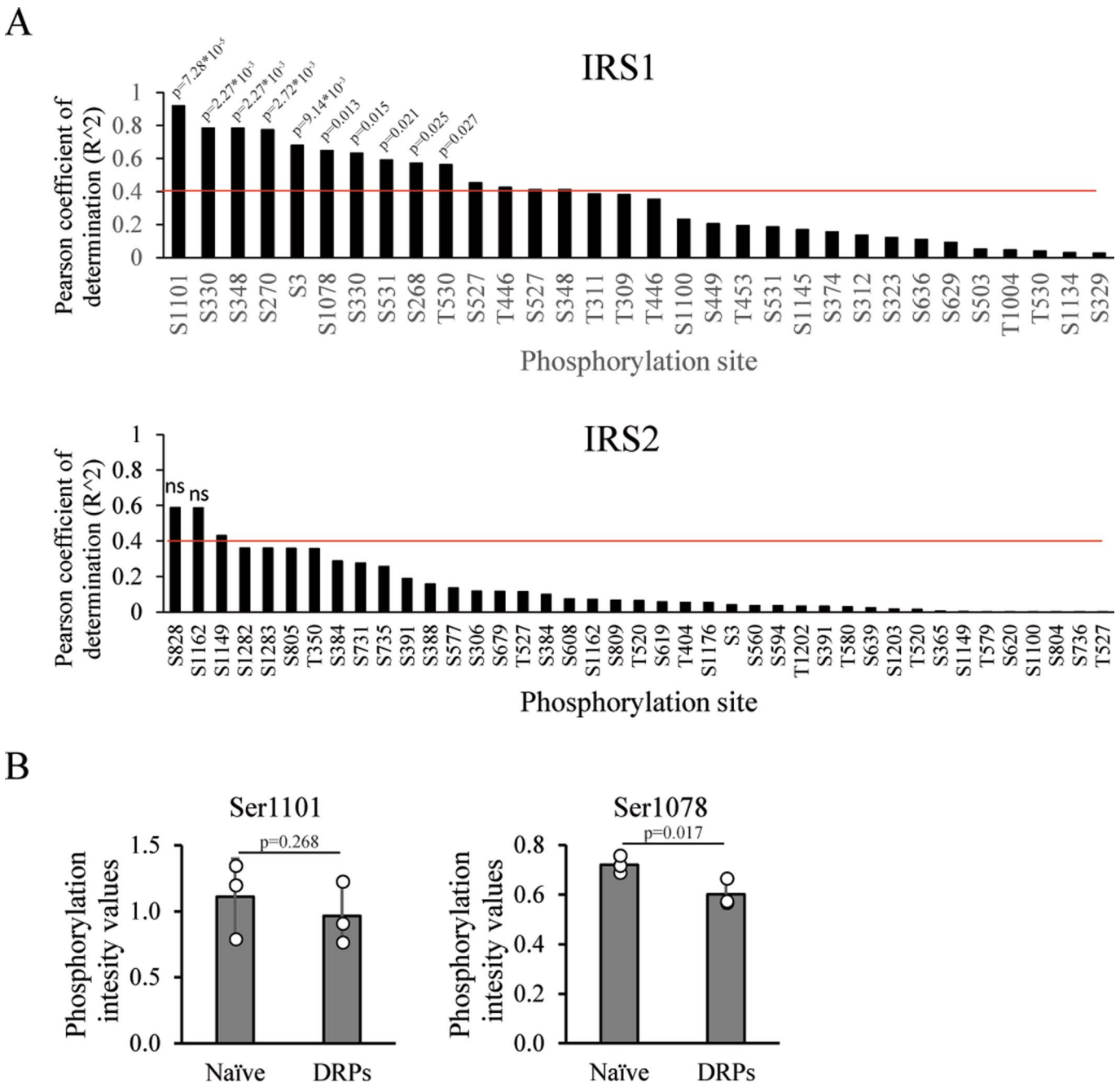

Extended Data Fig. 9 | IRS1 phosphorylation and response to therapy. (a) Pearson's correlation determination (r^2) test was used to calculate the correlation coefficient and the p-value between CTP and all detected phosphorylation sites in IRS1 (upper panel) and IRS2 (lower panel). The correlation was calculated based on n = 7 clones as well as the non-clonal PC9 population. FDR < 0.1 **(b)** pIRS1 (ser1101) and pIRS1 (ser1078) were measured in drug-naïve cells and DRPs of the G361 cell line treated 0.06 μM trametinib. Data are presented as mean values, error bars represent the standard deviation of n = 3 independent cultures. p-values were calculated by one tailed Student's *t*-test.

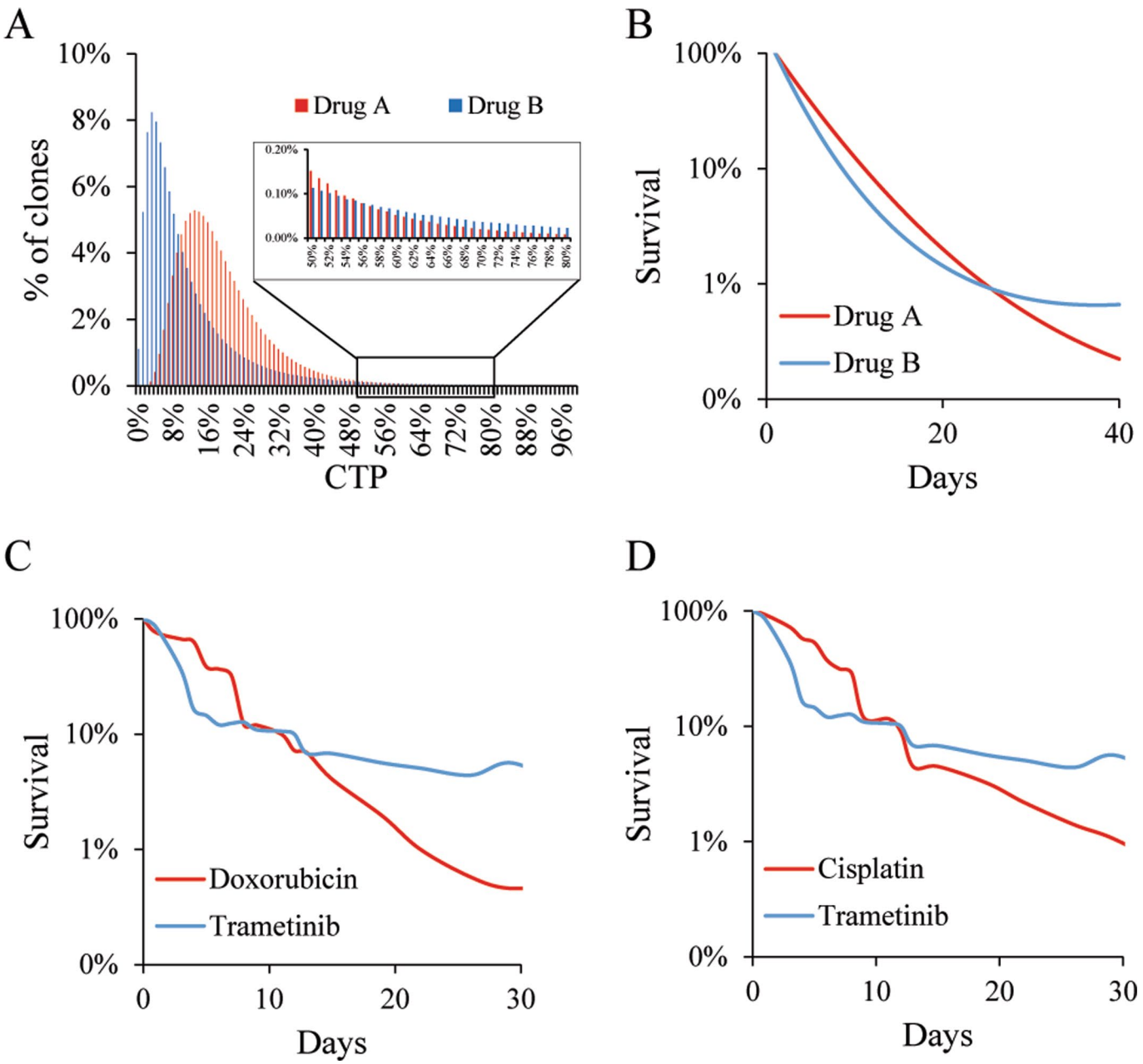

Extended Data Fig. 10 | CTP and the long term impact of competing treatments. While the mean CTP captures a treatment's short term impact, the complete CTP distribution, determines its long term effect. **(a)** Two competing hypothetical drugs (blue) and (red) are demonstrated. While the mean CTP of drug B (distribution peak) is smaller, indicating a rapid decline in the cancer cell population within the first week, the tail of this distribution is broader, and hence it exhibits a higher variance in CTP compared to drug A. **(b)** The calculated cell count, vs. time under the two treatments is presented. At day 7, drug B seems superior, however, as a result its broad tailed distribution, after approximately 2 weeks of treatment it becomes less effective than drug A. Such crossover illustrates the importance of the CTP *distribution*, as opposed to just the mean, as a predictor of treatment effectiveness. **(c)** An empirical example showing the cancer cell population under doxorubicin (blue) vs. trametinib (red). While the latter is three times more effective at day 7, the trend is reversed in later time points. **(d)** Similar crossover is observed for cisplatin vs. trametinib.

nature research

Corresponding author(s): Ravid Straussman

Last updated by author(s): 2021.07.15

Reporting Summary

Nature Research wishes to improve the reproducibility of the work that we publish. This form provides structure for consistency and transparency in reporting. For further information on Nature Research policies, see Authors & Referees and the Editorial Policy Checklist.

Statistics

For all statistical analyses, confirm that the following items are present in the figure legend, table legend, main text, or Methods section.

n/a	Confirmed
☐	☒ The exact sample size (*n*) for each experimental group/condition, given as a discrete number and unit of measurement
☐	☒ A statement on whether measurements were taken from distinct samples or whether the same sample was measured repeatedly
☐	☒ The statistical test(s) used AND whether they are one- or two-sided *Only common tests should be described solely by name; describe more complex techniques in the Methods section.*
☒	☐ A description of all covariates tested
☐	☒ A description of any assumptions or corrections, such as tests of normality and adjustment for multiple comparisons
☐	☒ A full description of the statistical parameters including central tendency (e.g. means) or other basic estimates (e.g. regression coefficient) AND variation (e.g. standard deviation) or associated estimates of uncertainty (e.g. confidence intervals)
☐	☒ For null hypothesis testing, the test statistic (e.g. *F*, *t*, *r*) with confidence intervals, effect sizes, degrees of freedom and *P* value noted *Give P values as exact values whenever suitable.*
☒	☐ For Bayesian analysis, information on the choice of priors and Markov chain Monte Carlo settings
☒	☐ For hierarchical and complex designs, identification of the appropriate level for tests and full reporting of outcomes
☐	☒ Estimates of effect sizes (e.g. Cohen's *d*, Pearson's *r*), indicating how they were calculated

Our web collection on statistics for biologists contains articles on many of the points above.

Software and code

Policy information about availability of computer code

Data collection	The Harmony software version 4.1 was used to image and count GFP-positive cells imaged by the Operetta automated imaging system (PerkinElmer).
Data analysis	Detailed explanation of data analysis was given in the methods section. In short - TopHat (version 2.0.10) algorithm was used to read alignment of bulk RNA-Seq reads. HTseq (version 0.6.1p1) was used for estimation of mRNA abundance. R package DEseq2 (version 1.6.3) algorithm was used for looking for differential expression. Quantification of western blots were done by ImageJ (version 1.53a). FlowJo version 10.7.1 was used for cell-cycle analysis by FACS. Raw MS files were analyzed by MaxQuant (version 1.5.3.36) with the integrated Andromeda search engine. The label-free quantification (LFQ) algorithm (version 1.5.3.36) was used in the proteome analysis. The code used in the manuscript (Extended Data 10) is available at https://doi.org/10.5281/zenodo.5036166

For manuscripts utilizing custom algorithms or software that are central to the research but not yet described in published literature, software must be made available to editors/reviewers. We strongly encourage code deposition in a community repository (e.g. GitHub). See the Nature Research guidelines for submitting code & software for further information.

Data

Policy information about availability of data

All manuscripts must include a data availability statement. This statement should provide the following information, where applicable:

- Accession codes, unique identifiers, or web links for publicly available datasets
- A list of figures that have associated raw data
- A description of any restrictions on data availability

The mass spectrometry phospho-proteomics data have been deposited to the ProteomeXchange Consortium via the PRIDE partner repository with the dataset identifiers PXD026824, PXD026842, PXD026844, PXD026857, PXD026805. The mass spectrometry proteomics data have been deposited to the ProteomeXchange Consortium via the PRIDE partner repository with the dataset identifier PXD026834. RNA-seq data that support the findings of this study have been deposited in the

Gene Expression Omnibus (GEO) under accession codes GSE178978 and GSE179240.

Field-specific reporting

Please select the one below that is the best fit for your research. If you are not sure, read the appropriate sections before making your selection.

☒ Life sciences ☐ Behavioural & social sciences ☐ Ecological, evolutionary & environmental sciences

For a reference copy of the document with all sections, see nature.com/documents/nr-reporting-summary-flat.pdf

Life sciences study design

All studies must disclose on these points even when the disclosure is negative.

Sample size	No calculations were done to determine sample size. In most experiments, three biological repeats (with additional technical repeats) were done to compare between groups (e.g. clones with differential CTP, effect of siRNA/over-expression etc.). To demonstrate the continuous nature of CTP we generated ~400-550 clones from each cell line. This number was determined by our technical ability. First RNA-Seq experiments were done on eight different clones and as no significant results were achieved we increased this number to 194 clones. Here again, the number 194 was determined by the technical feasibility that we had at this time.
Data exclusions	In the phospho-proteomics experiments samples with lower coverage than expected (= less than 7000 phospho-sites detected), were excluded from the analysis.
Replication	Both technical and biological replications were done. The number of the technical and biological repeats are depicted in the text and in the legend for each figure and sup. figure separately.
Randomization	Randomization was used in the MARS-seq library preparation and in the analysis of the phospho-proteomics samples as described in the methods.
Blinding	Blinding was used in assessment of viability and pIRS staining by an independent pathologist as described in the methods.

Reporting for specific materials, systems and methods

We require information from authors about some types of materials, experimental systems and methods used in many studies. Here, indicate whether each material, system or method listed is relevant to your study. If you are not sure if a list item applies to your research, read the appropriate section before selecting a response.

Materials & experimental systems

n/a	Involved in the study
☐	☒ Antibodies
☐	☒ Eukaryotic cell lines
☒	☐ Palaeontology
☐	☒ Animals and other organisms
☐	☒ Human research participants
☒	☐ Clinical data

Methods

n/a	Involved in the study
☒	☐ ChIP-seq
☐	☒ Flow cytometry
☒	☐ MRI-based neuroimaging

Antibodies

Antibodies used	pIGF1R (Tyr1165/1166) was purchased from Santa-cruz (#sc-135767) diluted 1:200. Anti pIRS1 ser1101 (LifeSpan BioSciences Inc; #LS-C352384, 1:100 dilution). phospho-ERK (Thr202/Tyr204) rabbit monoclonal Ab diluted 1:1000,pEGFR (Tyr1068) rabbit monoclonal Ab diluted 1:200, GAPDH rabbit monoclonal Ab diluted 1:10000 and HSP90 polyclonal Ab diluted 1:1000 were purchased from Cell Signaling (#4370, #3777, #2118, #4874). β-tubulin mouse monoclonal diluted 1:10000 was purchased from Sigma Aldrich (#SAB4200715). Anti-mouse secondary Ab and anti Rabbit secondary Ab were purchased from Li-Cor (#926-32211, #926-68070) both diluted 1:8000.
Validation	All antibodies used are commercially available. pIGF1R validation details can be found at: https://www.scbt.com/p/p-igf-ir-antibody-50-y1165-1166 pIRS1 validation details can be found at: https://www.lsbio.com/antibodies/irs1-antibody-phospho-ser1101-ihc-wb-western-ls-c352384/363505 pERK validation details can be found at: https://www.cellsignal.com/products/primary-antibodies/phospho-p44-42-mapk-erk1-2-thr202-tyr204-d13-14-4e-xp-rabbit-mab/4370 pEGFR validation details can be found at: https://www.cellsignal.com/products/primary-antibodies/phospho-egf-receptor-tyr1068-d7a5-xp-rabbit-mab/3777

Eukaryotic cell lines

Policy information about cell lines

Cell line source(s)	HCC2935 (#CRL-2869), G361 (#CRL-1424) and SKBR3 (#HTB-30) were purchased from the ATCC, EFM192A (#ACC 736) were purchased from DSMZ. The PC9 cell line was a gift from Dr. Channing Yu of the Broad Institute of Harvard and MIT.
Authentication	Cell-lines authentication by fingerprinting analysis was performed for SKBR3, PC9 (non clonal population) and two PC9 high CTP clones (Cl.4 and B12) to confirm their identity. HCC2935, G361 and EFM192A were not authenticated.
Mycoplasma contamination	All cell lines were tested negative for mycoplasma contamination by PCR.
Commonly misidentified lines (See ICLAC register)	No commonly misidentified lines were used in this study.

Animals and other organisms

Policy information about studies involving animals; ARRIVE guidelines recommended for reporting animal research

Laboratory animals	For the establishment of PDX models 6-week-old NOD/SCID mice were purchased from Harlan. For NSCLC study twenty 8 weeks old male NOD/SCID mice were purchased from the SPF unit, the faculty of medicine, Bar Ilan, Israel. For HNSCC study 7 weeks old female NOD/SCID mice were purchased from the SPF unit, the faculty of medicine, Bar Ilan, Israel.
Wild animals	No wild animals were used in the study.
Field-collected samples	No field collected samples were used in the study.
Ethics oversight	All procedures were performed under sterile conditions at the Faculty of Medicine, Bar Ilan University SPF facility, and carried out in accordance with the Guide for the Care and Use of Laboratory Animals of the National Institutes of Health and approved by the ethics committee of animal experiments of Bar Ilan University, Israel.

Note that full information on the approval of the study protocol must also be provided in the manuscript.

Human research participants

Policy information about studies involving human research participants

Population characteristics	NSCLC for ex-vivo organ culture (Fig. 5G) was obtained from Sheba medical center. Informed consent was obtained.
Recruitment	The patient was recruited by the surgeons involved in the study and was chosen depending only upon the availability of tissue and the willingness of the patients to participate in the study. Age, race, tumor location, presence of metastatsis, were not taken into consideration in choosing patients for the study.
Ethics oversight	The study was approved by the Sheba medical center IRB (protocol #SMC-4744) as well as by the Israeli ministry of health ethics committee (protocol #: 057-2007).

Note that full information on the approval of the study protocol must also be provided in the manuscript.

Flow Cytometry

Plots

Confirm that:

☒ The axis labels state the marker and fluorochrome used (e.g. CD4-FITC).

☒ The axis scales are clearly visible. Include numbers along axes only for bottom left plot of group (a 'group' is an analysis of identical markers).

☒ All plots are contour plots with outliers or pseudocolor plots.

☒ A numerical value for number of cells or percentage (with statistics) is provided.

Methodology

Sample preparation	Floating and adherent cells were collected and fixed overnight in 100% cold methanol. Cells were rehydrated in PBS for 30 min, followed by staining with Propidium Iodide (25µg/ml)/ RNAse A (50µg/ml).
Instrument	BD LSR II
Software	FlowJo version 10.7.1

Cell population abundance	Average of 76,544 single-cells out of total of 100,000 cells were analyzed.
Gating strategy	Single cells were gated according to PI-A/PI-H. Cell cycle phases were determined by the cell-cycle module of FlowJo program based on PI fluorescence.

☒ Tick this box to confirm that a figure exemplifying the gating strategy is provided in the Supplementary Information.